

Review

Review on Micro-Alloying and Preparation Method of 7xxx Series Aluminum Alloys: Progresses and Prospects

Yuxin Dai, Liangming Yan * and Jianpeng Hao

College of Materials Science and Engineering, Inner Mongolia University of Technology, Hohhot 010051, China; 20211000049@imut.edu.cn (Y.D.); jianpeng19980906@163.com (J.H.)

* Correspondence: yanliangming@126.com; Tel.: +86-13848106861

Abstract: Notably, 7xxx series aluminum alloy has become the most popular nonferrous alloy, extensively used in industry, construction and transportation trades, due to its high comprehensive properties such as high static strength, high strength, heat resistance, high toughness, damage resistance, low density, low quenching sensitivity and rich resource. The biggest challenge for aluminum alloy today is to greatly improve the corrosion resistance of the alloy, while maintaining its strength. The preparation method of 7xxx series aluminum alloy requires controlling time lapses in the process of heating, holding and cooling, and there are many species precipitates in the crystal, but the precipitated strengthening phase is a single type of equilibrium η' phase. Therefore, more attention should be paid to how to increase the volume fraction of η' precipitates and modify the comprehensive performance of the material and focus more on the microstructure of the precipitates. This article reviews the progress of 7xxx series aluminum alloy materials in micro-alloying, aging precipitation sequence, the strengthening-toughening mechanism and the preparation method. The effect of adding trace elements to the microstructure and properties of 7xxx series aluminum alloy and the problems existing in aging precipitation characteristics and the reinforcement mechanism are discussed. The future development direction of 7xxx series aluminum alloy is predicted by developing a method for the process-microstructure-property correlation of materials to explore the characteristic microstructure, micro-alloying, controlling alloy microstructure and optimizing heat-treatment technology.

Keywords: 7xxx series aluminum alloys; micro-alloying; aging precipitation sequence; strengthening-toughening mechanism; preparation method



Citation: Dai, Y.; Yan, L.; Hao, J. Review on Micro-Alloying and Preparation Method of 7xxx Series Aluminum Alloys: Progresses and Prospects. *Materials* **2022**, *15*, 1216. <https://doi.org/10.3390/ma15031216>

Academic Editor: Pavel Novák

Received: 17 November 2021

Accepted: 26 January 2022

Published: 6 February 2022

Publisher's Note: MDPI stays neutral with regard to jurisdictional claims in published maps and institutional affiliations.



Copyright: © 2022 by the authors. Licensee MDPI, Basel, Switzerland. This article is an open access article distributed under the terms and conditions of the Creative Commons Attribution (CC BY) license (<https://creativecommons.org/licenses/by/4.0/>).

1. Introduction

The first generation of 7xxx super-hard aluminum alloy was investigated in 1930, and developers are now looking at fifth generation aluminum alloy materials. Notably, 7xxx series aluminum alloy can be strengthened by heat-treatment and can achieve 490–820 MPa [1–5]. According to the addition of elements, alloys are mainly classified into two categories: Al-Zn-Mg alloy has exhibited better weldability and general corrosion resistance, and high strength can be obtained when heat treatment is appropriate; the other is developed on the basis of Al-Zn-Mg alloy by adding Cu, which has high specific strength, low density, yield strength close to tensile strength, and exhibits better corrosion resistance and high toughness. It is the highest strength series of aluminum alloy and is easy to machine, and is applied widely in large aircraft manufacturing and aerospace, and internationally recognized as the main aviation material [6–8]. In this paper, the new principle of process-microstructure-performance correlation is used to continuously improve the microstructure-performance characterization method of aluminum alloy, based on the composition-process-microstructure-performance relationship of 7xxx series aluminum alloy, which shows good prospects for the future development direction of aluminum alloy.

2. Micro-Alloying

After adding Zr, Mn, V, Cr and other micro-elements to 7xxx series aluminum alloy, the hardness of the alloy decreases and the hardenability decreases, in turn, during slow quenching. In this section, the effects of four kinds of elements on the properties of 7xxx series aluminum alloy are discussed, respectively. Table 1 summarizes the related properties of Al-Zn-Mg-Cu alloy.

Table 1. Summary of alloy elements on relevant properties of Al-Zn-Mg-Cu [3,6,8–18].

Element	Precipitate	Content ($\omega\%$)	Main Effect
Zn + Mg	η (MgZn_2); T ($\text{Al}_2\text{Mg}_2\text{Zn}_3$)	0.0–10 ($\text{Zn} \geq 0.9$)	Increased tensile strength; heat treatment effect
		$\text{Zn} + \text{Mg} \geq 10\%$	Decreased conductivity, fracture toughness, stress-corrosion resistance, and spalling-corrosion resistance
Mg	β (Al_8Mg_5)	0.0–4.0 ($\text{Mg} \geq 0.0$)	Reduced welding crack tendency
Mg + C	S (CuMgAl_2)	$\text{Zn}/\text{Mg} > 2.2$ $\text{Cu} > \text{Mg}$	Improved alloy strength
Cu	θ (CuAl_2)	≤ 3	Improved corrosion resistance
			Expanded the stable temperature range of GP zone, improved the tensile strength, plasticity and fatigue strength
Cr	Incoherent E ($\text{Al}_{18}\text{Cr}_2\text{Mg}_3$)	≤ 0.35	Nucleation and precipitation of coarse equilibrium phase
	(CrMn) Al_{12} ; (CrFe) Al_7	0.1–0.2	Fine grain strengthening; inhibits recrystallization nucleation and growth; Improve anti SCC ability
Mn	Al_6Mn	0.2–0.4	Improved maximum tensile strength and fracture toughness, performance of low cycle fatigue, quenching sensitivity
	$\text{Al}_{20}\text{Cu}_2\text{Mn}_3$	> 0.4	Reduced the number of strengthening phases
Zr	Al_3Zr	0.05–0.16	Improved the strength, toughness, aging effect and corrosion resistance of the alloy
Ag		0.16	Promoted the formation of GP region and transition phase; delayed the over-aging of the alloy
Co	(Co,Fe) Al_9 , Co_2Al_9	$0.05 \leq \geq 0.2$	Improved the hardenability; retention of subcrystalline structure
Ti		0.01–0.08	Refined grain, improved casting properties
Er	Al_3Er ; $\text{Al}_8\text{Cu}_4\text{Er}$	0.1–0.15	Improved the toughness; hardenability; dimples appear
Sc	Al_3Sc	0.1–0.4	Grain refinement; recrystallization inhibition
Sc + Zr	$\text{Al}_3(\text{Sc,Zr})$	0.6	Improved anti SCC ability
Y	Al_3Y	0.3	Improved the hardness, tensile strength, elongation
Gd	$\text{Al}_3(\text{Gd,Zr})$	0.11	Hindered dislocation; grain boundary movement
Si	Mg_2Si ; AlFeMnSi	≥ 0.15	Reduced plasticity and fracture toughness
Fe	Al_6FeMn	≥ 0.15	Reduced plasticity and fracture toughness

2.1. Main Alloy Elements

In Al-Zn-Mg alloy, Zn and Mg are the main alloy elements, comprising not more than 7.5%. With the increase in Zn and Mg content, the ultimate tensile strength and heat treatment effect improved. When the content of $\text{Mg} + \text{Cu} \leq 7\%$, the alloy exhibits better stress-corrosion resistance, and the welding crack tendency decreases with the increase in Mg. The main function of the Cu element in Al-Zn-Mg-Cu alloy is to improve the corrosion resistance of the material, and the Cu element also has a certain enhancement effect [19]. Zn and Mg will form η (MgZn_2) phase and T ($\text{Al}_2\text{Mg}_2\text{Zn}_3$) phase after co-existence and aging. Mg/Zn mass ratio in the range of 5:2–7:1 can refine the precipitates and improve

the strength of the alloy; when the content of Zn + Mg \geq 10%, the electrical conductivity, fracture toughness, stress-corrosion resistance and exfoliation corrosion resistance of the alloy begin to decrease [20].

When the content of Zn/Mg $>$ 2.2 and Cu $>$ Mg, the strengthening phase S (CuMgAl₂) can enhance the strength of the alloy. The increase in Cu content will promote the recrystallization of the alloy, increase the density of the precipitated phase, and reduce the potential difference between the grain boundary and the grain [21]. The effect on PFZ (precipitation free zone) width is small, and the stress-corrosion resistance of the alloy is improved. If the element ratio is not within this range, S phase is the brittle phase that destroys the properties of the alloy. The size difference between the Cu atom and the Al atom is quite distinct; consequently, the crystal lattice deformation of Cu dissolved in Al-based solid solution in the form of replacement solid solution will reduce the hardenability of aluminum alloy and promote the precipitation of second phase in quenching [22]. In the process, the aging strengthening effect is reduced, and the quenching sensitivity of the alloy is reduced. The artificial aging process of the alloy in the range 100–200 °C is accelerated, expanding the stable temperature range of the GP (pre-dissolved atomic segregation area) region and improve the ultimate tensile strength, plasticity and fatigue strength. However, the addition of Cu tends to produce intercrystalline corrosion and pitting corrosion. The commonly used chemical composition of 7xxx series aluminum alloys is shown in Table 2 [20,21,23–26]. In addition to the main alloy elements such as Zn, Mg and Cu, there are also minor Mn and Cr elements that not only form new strengthening phases with the main alloy elements to increase the alloy strength, but also simultaneously improve the thermal strength and corrosion resistance.

Table 2. 7xxx series aluminum alloy grade and main chemical composition (w%) [20,21,23–26].

Alloys	Si	Fe	Cu	Mn	Mg	Cr	Zn	Ti	Zr	Other		Al
										Each	Total	
7A01	0.30	0.30	0.01	-	-	-	0.9–1.3	-	-	0.03	-	Bal.
7A03	0.20	0.20	1.8–2.4	0.10	1.2–1.6	0.05	6.0–6.7	0.02–0.08	-	0.05	0.10	Bal.
7A04	0.50	0.50	1.4–2.0	0.20–0.60	1.8–2.8	0.10–0.25	5.0–7.0	0.10	-	0.05	0.10	Bal.
7A05	0.25	0.25	0.20	0.15–0.40	1.1–1.7	0.05–0.15	4.4–5.0	0.02–0.06	0.10–0.25	0.05	0.15	Bal.
7A09	0.50	0.50	1.2–2.0	0.15	2.0–3.0	0.16–0.30	5.1–6.1	0.10	-	0.05	0.10	Bal.
7A10	0.30	0.30	0.50–1.0	0.20–0.35	3.0–4.0	0.10–0.30	3.2–4.2	0.10	-	0.05	0.10	Bal.
7A19	0.30	0.40	0.08–0.30	0.30–0.50	1.3–1.9	0.10–0.20	1.5–5.3	-	0.08–0.20	0.05	0.15	Bal.
7A33	0.25	0.30	0.25–0.55	0.05	2.2–2.7	0.10–0.20	4.6–5.4	0.05	-	0.05	0.10	Bal.
7A52	0.25	0.30	0.05–0.20	0.20–0.50	2.0–2.8	0.15–0.25	4.0–4.8	0.05–0.18	0.05–0.15	0.05	0.15	Bal.
7003	0.30	0.35	0.20	0.30	0.50–1.0	0.20	5.0–6.5	0.20	0.05–0.25	0.05	0.15	Bal.
7020	0.35	0.20	0.20	0.05–0.50	1.0–1.4	0.10–0.35	4.0–5.0	-	0.08–0.20	0.05	0.15	Bal.
7022	0.50	0.50	0.50–1.0	0.10–0.40	-	0.10–0.30	4.3–5.2	-	-	0.05	0.15	Bal.
7050	0.12	0.15	2.0–2.6	0.10	1.9–2.6	0.04	5.7–6.7	0.06	0.08–0.15	0.05	0.15	Bal.
7075	0.40	0.50	1.2–2.0	0.03	2.1–2.9	0.18–0.28	5.1–6.1	0.02	-	0.05	0.15	Bal.
7475	0.10	0.12	1.2–1.9	0.06	1.9–2.6	0.18–0.25	5.2–6.2	0.06	-	0.05	0.15	Bal.

2.2. Microalloying Elements

Adding microcontent of Zr, Mn, Cr, Ag elements in 7xxx series aluminum alloy can not only improve the recrystallization temperature of the alloy, but also refine crystal grain, thus giving the alloy high mechanical properties and anti-corrosion capacity.

2.2.1. Zr and Mn Transition Elements

Fang et al. [24] found that the addition of Zr (0.1~0.15%) in 7xxx series aluminum alloy can form Al₃Zr dispersion phase with significant strengthening effect on the alloy. The pinning effect of Al₃Zr on the grain boundary can inhibit the recrystallization and grain growth behavior of the alloy, and improve the yield strength, tensile strength and elongation of the alloy. Due to the extremely low solubility of Zr in aluminum, Al₃Zr particles are easily precipitated with the addition of microcrystalline Zr element. It is concluded that Al₃Zr is a small particle dispersed in the grain and on the crystal boundaries, which is beneficial to

refine the alloy grain, improve the strength, toughness, aging effect and corrosion resistance of the alloy.

There are only three ways for Zr to exist in aluminum alloy [25]: (1) Solid solution in the matrix; (2) In the process of solid solution or homogenization, coherent or incoherent Al_3Zr (D0_{23}) dispersion particles are released from the supersaturated solid solution, which acts as dispersion strengtheners; (3) During the melting process, Zr element segregates from the matrix, resulting in the formation of Al_3Zr primary crystals with coarse size, which is not conducive to the alloy's performance.

Md Shahnewaz et al. [27] found that the addition of Mn in 7xxx series aluminum alloy forms Al_6Mn particles improves the stress-corrosion resistance of the alloy. Al_6Mn does not affect the width of PFZ and can increase the maximum tensile strength, fracture toughness, and simultaneously improve the low cyclic fatigue performance. Valeev SH I et al. [28] pointed out that excessive Mn content would lead to the emergence of $\text{Al}_{20}\text{Cu}_2\text{Mn}_3$ and other second-phase compounds in aluminum alloys, which reduced the number of strengthening elements and strengthening phases in aluminum alloys, and the quenching sensitivity increased with the excess level of Mn content.

2.2.2. Cr and Ag Microalloying Elements

Notably, 7xxx series aluminum alloy has strong quenching sensitivity, and it is difficult to prepare rather thick plates with consistent strength [8,29]. If Zr is substituted with Cr, the quenching sensitivity can be greatly reduced and the effect of Cr on inhibiting recrystallization of 7xxx series aluminum alloy can be retained. Many investigations have shown that [24,30–32]: Cr element can form fine second phases of intermetallic compounds such as E ($\text{Al}_{18}\text{Cr}_2\text{Mg}_3$) phase, $(\text{CrMn})\text{Al}_{12}$ and $(\text{CrFe})\text{Al}_7$ in aluminum alloy, which can effectively prevent the recrystallization nucleation and growth of aluminum alloy during processing. Micro amounts of Cr will improve the stress-corrosion resistance of aluminum alloy, and it will combine better with Cu. Generally, the content of Cr in aluminum alloy is 0.1–0.2%. However, in recent years, due to the better comprehensive performance of dispersion particles generated by Zr and other elements or aluminum matrix, Zr is used to replace Cr.

Adding minor Ag (0.16%) to Al-Zn-Mg-Cu-Zr alloy disclosed that Ag could promote the formation of GP zone and transition phase [33], improve the stability of transition phase, delay the over-aging of the alloy, and thus improve the thermal stability of aluminum alloy [34]. Figure 1 XRD shows that the addition of Ag element in 7xxx series aluminum alloy does not change the main phase composition.

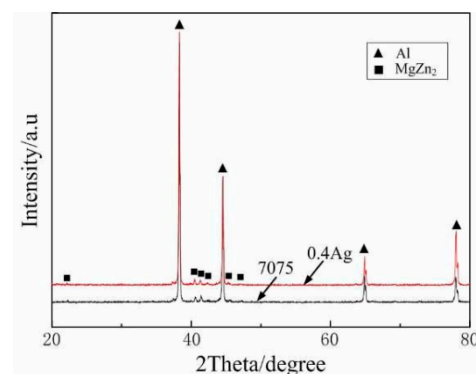


Figure 1. XRD pattern of as-cast 7075 (0 Ag) alloy and 0.4 Ag alloy. Adapted with permission from ref. [34]. 2015 Xu.

Figure 2 shows the rolled structure of the alloy with different content of the Ag element. After homogenization treatment and rolling deformation of 7075 alloy, it can be seen that the grains become longer along the rolling direction. After homogenization treatment, there

are still superior second phases around the grains. The second phase of the alloy containing Ag is less than that of the alloy without Ag, and the aggregation phenomenon is weakened.

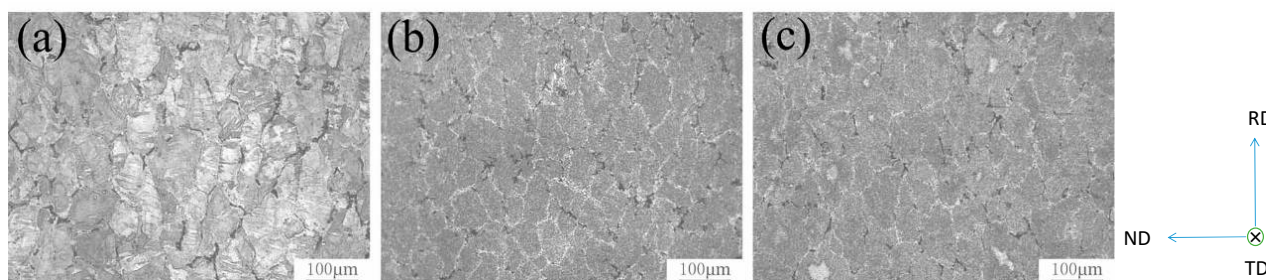


Figure 2. Microstructure of rolled alloys with different compositions: (a) 0 Ag (7075), (b) 0.2 Ag and (c) 0.4 Ag. Adapted with permission from ref. [34]. 2015 Xu.

2.3. Rare Earth Elements

There are 17 rare earth elements, which are the third subfamily of the periodic table. The addition of rare earth elements can purify, modify, micro alloy, and strengthen and improve the electrical conductivity of aluminum alloys. Depending on the different performance needs of aluminum alloys, the mass fraction of rare earth elements in the range of 0.1–0.4% is the best proportion [35]. Table 3 [20,24,36–38] explains the characteristics of the main rare earth elements in aluminum.

Table 3. Properties of major rare earth elements and their properties in aluminum [20,24,36–38].

Element	HV	Atomic Radius (nm)	Relative Difference with Al Atomic Radius (%)	Electronegativity	Electronegativity Difference with Al	Melting Point of Pure Aluminum and Eutectic Temperature Difference (°C)	Eutectic POINT Composition (w(RE)%)
Er	700	0.1757	23	1.2	0.3	5	1
Sc	850	0.1641	14.8	1.3	0.2	5	0.3
Y	600	0.1803	26.2	1.2	0.3	10	3.3
La	400	0.1877	31.4	1.1	0.4	20	2.5
Ce	250	0.1824	27.6	1.05	0.45	20	2
Nd	350	0.1522	27.5	1.2	0.3	20	7.4
Sm	450	0.1802	26.1	1.2	0.3	28	1.5
Eu	-	0.2041	42.8	1.1	0.4	-	-
Gd	550	0.1801	26	1.2	0.3	17	2
Tb	600	0.1783	24.8	1.2	0.3	16	1.8
Dy	550	0.1775	24.2	1.2	0.3	24	8.2
Ho	600	0.1767	23.7	1.2	0.3	13	2.6
Tm	650	0.1747	22.3	1.2	0.3	16	1.7
Yb	250	0.1939	35.7	1.1	0.4	35	4

It can be discerned from Table 3 that the difference between the melting point of pure aluminum and the eutectic temperatures of rare earth elements Er and Sc is relatively low, and the eutectic point composition of Sc is the lowest, $w(\text{Sc})\% \approx 0.3\%$, $w(\text{Er}) \approx 1.0\%$. Therefore, it can be perceived that the properties of 7xxx series aluminum alloy with the addition of Sc will be remarkably improved.

2.3.1. Er

Liu et al. [39] identified the effect of rare earth element Er on the failure behavior of 7xxx series aluminum alloy. The results show that the addition of Er can enhance the strength of 7xxx series alloy. When Zr and rare earth elements coexist, the performance of the alloy gets better. When the mass fraction of Zr is 0.14%, Er has a strong ability to improve strength (4.2%). When the mass fraction of Zr is 0.27%, Er has a weak ability to improve strength (3.1%); a trace addition of Er can improve the plasticity of the material; the fracture mechanism of the alloy without Er is brittle fracture, and secondary cracks

appear. The toughness of the alloy with a trace addition of Er is enhanced, and dimples appear, which changes from brittle fracture to ductile fracture mode [40].

2.3.2. Sc

Due to the decrease in the recrystallization fraction and the discontinuous distribution of GBPs, 0.06 wt% Sc added to medium strength Al-Zn-Mg alloy has excellent SCC resistance under aging conditions [41]. Excessive addition of 0.11 wt% Sc can increase the electrochemical activity and hydrogen embrittlement rate of GBPs and PFZ, thereby reducing the SCC resistance of the alloy.

Figure 3 exhibits the peak SCC sensitivity index (ISCC) of the three alloys. Figure 4 shows the SCC crack growth path diagram of the three alloys. Due to the decrease in the recrystallization fraction and the discontinuous distribution of GBPs, 0.06 wt% Sc added to medium strength Al-Zn-Mg alloy has superordinary SCC resistance and excellent mechanical properties, even under aging conditions. Excessive addition of 0.11 wt% will increase the electrochemical activity and hydrogen embrittlement rate of GBPs and PFZ, and reduce the SCC resistance of the alloy.

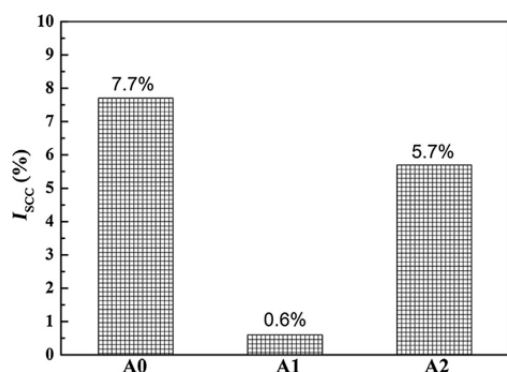


Figure 3. SCC susceptibility index (ISCC) of three peak-aged alloys. For Al Zn Mg alloys with 0 wt% Sc (A0), 0.06% Sc (A1) and 0.11% SC (A2)After homogenization treatment (470 °C for 24h), the ingot is preheated at 450 °C for 1H. Adapted with permission from ref. [41]. 2018 Li et al.

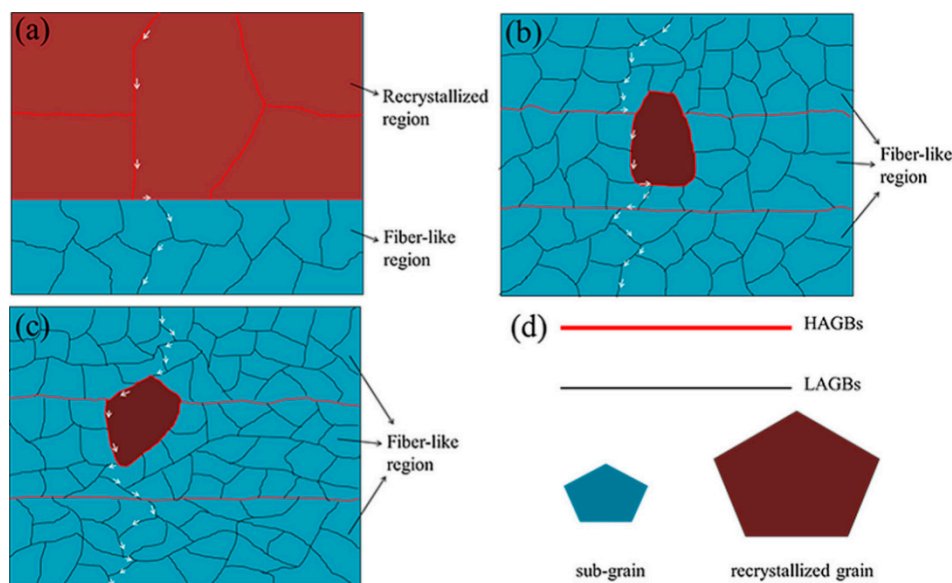


Figure 4. Schematization of SCC crack propagation paths for three peak-aged alloys: (a) A0; (b) A1; (c) A2; (d) the type of GB and grain. Adapted with permission from ref. [41]. 2018 Li et al.

2.3.3. Sc and Zr

The addition of trace amounts of Sc and Zr in Al Zn-Mg-Cu alloy is more beneficial for improving the extremely fine Al_3 (Sc, Zr) particles, and the alloy obtains higher strength and ductility, because the dispersed Al_3 (Sc, Zr) particles with L_{12} structure are formed during homogenization. Al_3 (Sc, Zr) particles with L_{12} structure precipitates at any time into coherent Al_3 (Sc,Zr) particles with D_{023} structure. L_{12} structure precipitated can effectively hinder recrystallization, inhibit grain growth, and improve the mechanical properties of the alloy [42]. Sc is a transitional element in rare earth elements and has been used as a kind effective grain refiner to replace Ti/TiB. Primary Al_3Sc particles can be used for excellent heterogeneous nucleation and can effectively refine the grain size of aluminum alloy during solidification. In the Al–Sc binary system, the recrystallization can be effectively retained by adding between 0.15 and 0.20% Sc. Xiao et al. [43] found that compared with the addition of 0.10% Zr, the alloy with 0.07% Sc and 0.07% Zr can resist recrystallization more effectively and improve the mechanical properties of 7xxx series aluminum alloy.

2.3.4. Y

In recent years, it has been found that a small amount of Y can refine the secondary dendrites of 7xxx alloy, reduce the size of eutectic compounds and improve the impact toughness of the alloy. According to the composition of the main alloy elements, Al_3Y , $\text{Al}_6\text{Cu}_6\text{Y}$ or $\text{Y}_{12}\text{Al}_3\text{Zn}$ rare earth compounds will be formed, which have an obvious effect on grain refinement. Li et al. [44] found that after adding 0.25 Er and 0.15 Y to 7xxx series aluminum alloy, the dissolution temperature of eutectic compound increased, the nucleation rate increased, and the fine grain strengthening was achieved. Table 3 points out that the atomic radius difference between the Y atom and the Al atom is 26%. The deformation mechanism of Y in 7xxx series aluminum alloy is that when the Y atom enters the aluminum alloy, the lattice distortion and the free energy of the alloy increase, and the rare earth phase compounds containing Y can only be distributed at the grain boundary. Furthermore, when Y enters the alloy, the second phase at the grain boundary increases, which inhibits the growth of grains. The generated Al_3Y , $\text{Al}_6\text{Cu}_6\text{Y}$ or $\text{Y}_{12}\text{Al}_3\text{Zn}$ rare earth compounds as the core of heterogeneous nucleation can strengthen the aluminum alloy. If the rare earth element Y is excessive, the second phase will be enriched, and the comprehensive properties of the alloy will be greatly reduced. Due to the low price of rare earth element Y, it is an important additive element with potential for future development.

2.3.5. Gd

The rare earth element Gd also has a certain influence on the high temperature properties of the alloy. The addition of rare earth element Gd to the 7xxx series aluminum alloy forms a uniformly distributed L_{12} -type Al_3 (Gd, Zr) dispersed phase, rather than a core-shell-shaped Al_3 (Sc, Zr) dispersed phase produced by adding Sc element to the 7xxx series aluminum alloy. Chen et al. [45] found that the addition of 0.11% Gd in 7xxx series aluminum alloy has a significant effect on hindering dislocation and grain boundary movement, stabilizing a large number of deformation and recovery structures of fine sub-grain boundaries. The stress-corrosion crack propagation rate of the alloy was effectively delayed. The addition of 0.11% Gd element to 7056 aluminum alloy also increased the KI (critical stress intensity factor) of 7056 from $5.45 \text{ MPa}\cdot\text{m}^{1/2}$ to $10.59 \text{ MPa}\cdot\text{m}^{1/2}$.

Mei et al. [46] identified, as shown in the Figure 5, that after high temperature solution treatment, the alloy without Gd added fully recrystallized, forming equiaxed recrystallized grains, and the alloy with Gd added still maintains fine fibrous unrecrystallization microstructure, indicating that the formed dispersion phase can effectively hinder the transformation of deformation-recovery microstructure to sub-grain microstructure, thereby inhibiting the recrystallization of the matrix. This shows that the rare earth element Gd is mainly distributed among dendrites in 7075 aluminum alloy with Al_3Gd compound.

Adding Gd within the effective range can improve the tensile strength and elongation of aluminum alloy.

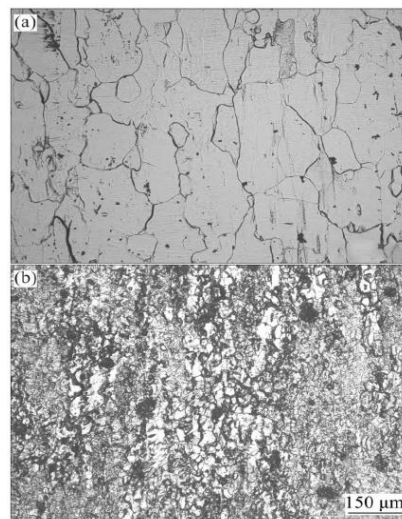


Figure 5. Optical microstructures of the two studied alloys with solution treatment: (a) 0% Gd and (b) 0.25% Gd. Adapted with permission from ref. [46]. 2012 Mei et al.

2.4. Non-Metallic Inclusions Element

Fe and Si elements are harmful impurities in 7xxx series aluminum alloys. The main phases of impurity elements Fe and Si in 7xxx series aluminum alloys are brittle phases such as Al_7Cu_2Fe , $MgSi_2$, $AlFeMnSi$ and eutectic compounds [20,24]. Due to the impurity particles containing Fe and Si being distributed inside the grains or on the grain boundaries, and they are difficult to dissolve at high temperature, it easily produces the banded structure that is arranged intermittently along the deformation direction during hot deformation. In the process of plastic deformation, due to the uncoordinated deformation of the brittle phase matrix, microcracks are easily generated on some grain-matrix boundaries and become the source of macroscopic cracks, which have an unfavorable influence on the plasticity and fracture toughness of the alloy. At present, the mass fraction of Fe and Si impurities in 7xxx series aluminum alloys should be limited to below 0.15% [20,24].

3. Aging Precipitation Sequence and Strengthening-Toughening Mechanism of 7xxx Series Aluminum Alloy

The main phases that can be brought about between the elements of Al-Zn-Mg-Cu quaternary alloy mainly include α phase (Al matrix), θ phase ($CuAl_2$), S phase (Al_2CuMg), η phase ($MgZn_2$), β phase (Al_8Mg_5) and T phase ($Al_2Mg_2Zn_3$). The precipitated phases affect the main properties of the material [47].

3.1. Precipitated Sequence

Figure 6 [48] shows the temperature dependence of Al-rich angle of equilibrium phase in 7xxx series aluminum alloys. According to the phase diagram, the increase in Cu content promotes the appearance of θ phase. When the Cu content is lower, the phase composition is mainly affected by the Zn/Mg ratio. When the Zn/Mg ratio is extremely small, all the amounts are composed of $\alpha + S + T$ phase or medium $\alpha + T$ phase without η phase; when the Zn/Mg ratio increased, η phase began to appear and gradually increased, accompanied by S phase and T phase.

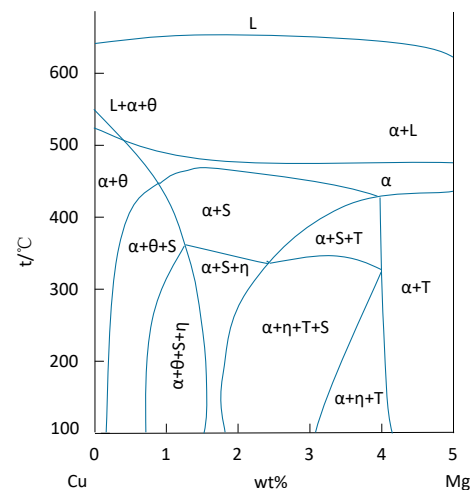


Figure 6. Variable temperature section of aluminum rich angle of equilibrium phase of 7xxx series aluminum alloy. Adapted with permission from ref. [48]. 2018 Zhang and Deng.

The precipitation sequence of precipitates in 7xxx series aluminum alloy is classified into three types: the first is GP zone (supersaturated solid solution SSS \rightarrow GP I zone \rightarrow GP II zone \rightarrow η' phase \rightarrow η phase); the second is when the Mg content is high, supersaturated solid solution SSS appears in defects and grain boundaries, the precipitation order is: (supersaturated solid solution SSS \rightarrow T phase and macroscopic Al-Zn-Mg-Cu phase \rightarrow η phase); finally, when the supersaturated solid solution SSS appears in the vacancy-rich region, the precipitation order is (SSS \rightarrow VRC (vacancy-related cluster) vacancy enrichment \rightarrow T phase and coarse Al-Zn-Mg-Cu phase \rightarrow η phase). The three kinds of different precipitation behavior eventually formed a stable η phase; the precipitation order is shown in Figure 7 [48]. The main strengthening phases of Al-Zn-Mg-Cu alloy include GP zone and η' phase. The GP zone is a fully coherent Mg and Zn enrichment zone with the aluminum matrix, which is spherical (GP I zone) or strip (GP II zone), while the η' phase is a hexagonal plate metastable phase, semi-coherent with the aluminum matrix, which is the uppermost aging strengthening phase. The η phase is a disc-shaped equilibrium phase that is not coherent with the matrix [49]. If there is T phase under certain composition conditions, η phase will be replaced by T phase. Due to the existence of Cu atoms in the alloy, the S phase will appear at the grain boundaries at a certain Zn/Mg ratio. It will act as a cathode to continuously dissolve the surrounding matrix to form pitting corrosion, which will also lead to poor fracture properties of aluminum alloys. Table 4 summarizes the main precipitated phases and their structure characteristics in 7xxx series aluminum alloys [1,6,48,49].

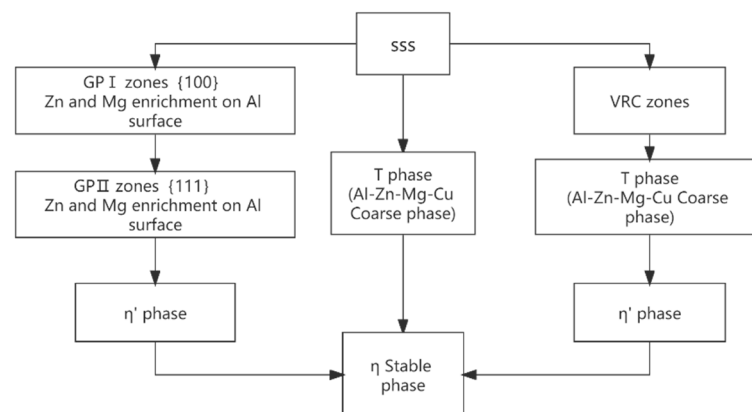


Figure 7. Precipitation sequence of precipitates in 7xxx series aluminum alloy. Adapted with permission from ref. [48]. 2018 Zhang and Deng.

Table 4. Morphology and structure characteristics of main precipitates in 7xxx series aluminum alloy [50–54].

Precipitation	Crystal Structure	Lattice Constant/nm			Morphology And Crystal Orientation	Precipitation Temperature/°C
		a	b	c		
H' (MgZn ₂)	Hexagonal system (L1 ₂)	0.496	-	1.403	semi-Coherent, (0001) _{η'} //{111} _{Al} ; (11-20) _{η'} //<112> _{Al} ; (10-10) _{η'} //(110) _{Al} ; habit plane(111) _{Al}	120–250
Metastable phase η _p (Al ₂ Mg ₂ Zn ₈)	Hexagonal system	0.496	-	0.935	semi-Coherent, (0001) _{η_p} //{111} _{Al} ; (11-20) _{η_p} //<112> _{Al} ; (10-10) _{η_p} //(110) _{Al}	300–400
T' (Al ₂ Mg ₂ Zn ₃)	Cubic system	500	-	-	Incoherent; Equiaxed Polytopic	471–476
S' (Al ₂ CuMg)	Orthorhombic system	0.4012	0.9265	0.7124	Incoherent; Bar shape	456–482
η (MgZn ₂)	(D0 ₂₃)	0.516–0.522	-	0.849–0.855	Incoherent; 13 orientation relationship; classic orientation relationship (0001) _η //{111} _{Al} ; (10-10) _η //(110) _{Al}	150–476
Stable phase S (Al ₂ CuMg)	Orthorhombic system	0.4	0.025	0.715	semi-Coherent	400–494
T (Al ₂ Mg ₂ Zn ₃)	Cubic system	1.416	-	-	Coherent, (060) _T //(111) _{Al} ; (103) _T //(2-20) _{Al}	Low temperature precipitation: 174
θ (CuAl ₂)	Tetragonal system	0.607	-	0.487	Coherent	451; Low temperature precipitation: 80

According to the crystallography theory [11,55], there are four equivalent variants of η phase on the Al plane. As shown in Figure 8a, four disk η phases with the same thickness and diameter keep their (0001)_η habit planes parallel to four equivalent {111}_{Al} planes, which are defined as V1–V4 variants. Figure 8b shows that V1 and V2 variants are marginal, while V3 and V4 variants are elliptical, as observed in the direction [110]_{Al}. It can be seen from Figure 8 that when the temperature is lower than 100 °C, the η precipitates in the alloy are mainly V3 and V4. When the temperature range is 125–175 °C, V1 and V2 mainly contain η precipitates [55].

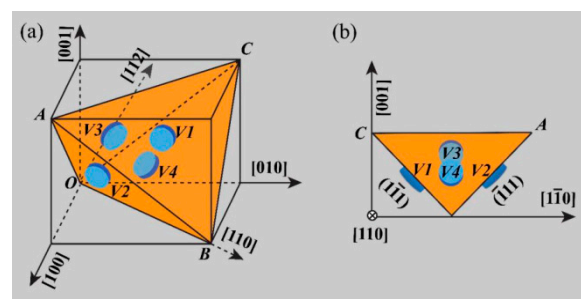


Figure 8. Schematic illustrations showing four types of η variants V1-4 on {111}_{Al} (a) The three-dimensional view, and (b) the projection from [110]_{Al} direction. Adapted with permission from ref. [55]. 2021 Zang et al.

Figure 9a shows that η' phase is thin margin (elongated) on {111}_{Al} plane. The insertion of the upper left corner shows the fast fourier transform (FFT) pattern diagram of the η'

phase with weak scattering. When the temperature reaches 175 °C, Figure 9e, η' thickness and radius increase, respectively. A larger radius and thickness of η precipitates can also be observed. The clearer observation results in Figure 9g show the obvious aboriginal lattice distortion caused by the incoherence between η phase and α -Al matrix.

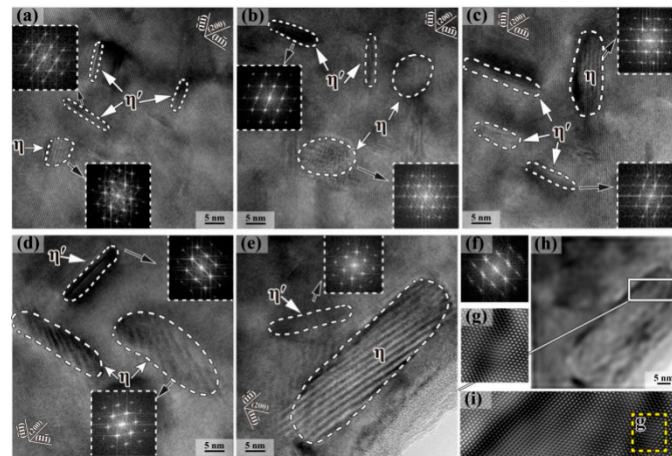


Figure 9. HRTEM images of the precipitates viewed along $\langle 110 \rangle$ Al orientation in 7085 alloy after various heat treatments: (a) sample I (25 °C); (b) sample II (100 °C); (c) sample III (125 °C); (d) sample IV (150 °C); (e) sample V (175 °C); (f) corresponding FFT pattern of η phase in (e); (g) is from the yellow dashed frame in (i); (h) is the corresponding inverse FFT image of (e), and; (i) is from the white solid frame in (h). Adapted with permission from ref. [55]. 2021 Zang et al.

Khalfallah et al. [56] found by DSC that the formation of GP region is controlled by the migration of Zn and Mg atoms, while η' metastable and η precipitation of stable phase is affected by the migration and diffusion of solute atoms. Berg et al. [57] found that GP I region was formed in a wide temperature range from room temperature to 140–150 °C, and was independent of quenching temperature. These regions are consistent with the aluminum matrix. Based on the $\text{AlCu}_{(1)}$ type subunit, the interior of the matrix lattice is arranged as Zn and Al or Mg, and the periodic inverse boundary is formed after quenching above 450 °C and aging above 70 °C. According to the diffraction theory, the GPII region is identified as a Zn-rich layer on the $\{111\}$ plane, the inside of which is arranged in a slender crystal orientation. The habit plane of GPII region is the $\{111\}$ plane, indicating that not all GP regions can be transformed into η' phase. The η' phase is seven-layer $\{111\}_{\text{Al}}$ thick, with O (orthorhombic) and R (rhombohedral) subunit units inside. Each ligand is formed by the push-ring contact between two atoms and six atoms. It can be seen that the GP zone with smaller size has higher surface energy, which is more unstable than the GP zone with larger size. With the aging process, the GP zone with smaller size is transformed into η' phase. Figure 10 [58] shows the lattice and crystal structure of 7xxx series aluminum alloy under haddf-stem.

3.2. Strengthening and Toughening Mechanism

3.2.1. Strengthening

The strengthening and toughening of 7xxx series aluminum alloy deformation mainly includes solid solution strengthening, second phase strengthening, grain boundary strengthening and processing strengthening. The existing problem is still that the comprehensive performance of strength and toughness and stress-corrosion resistance are low. According to the aging precipitation [55,59–62], the phase, GBPs and PFZ of the precipitated alloy after aging determine the properties of the aluminum alloy. Reducing the slip of the eutectic surface and narrowing the PFZ of the grain boundary, optimizing the composition design of the alloy and improving the heat treatment method are the specific means to improve the comprehensive properties of the alloy [46]. Improving the properties of the aluminum alloy

cannot only start from the composition design, but also must understand the performance theory and characterization method of the microstructure in depth [63]. Dai et al. [64] researched the mechanical properties of 7xxx series aluminum alloy at 470 °C under different solution times. With the extension of solution holding time, the tensile strength and elongation of the alloy increased first to the peak and then decreased gradually. Under 470 °C solution state, the tensile strength and yield strength of the alloy were the highest when the aging time was 120 min, which were 475.3 MPa and 448.6 MPa, respectively. After solution treatment and aging at 120 °C for 24h, the tensile strength reached a peak of 613.5 MPa at 120 min, and the yield strength reached a peak of 578.5 MPa at 160 min. Figure 11 shows the changes of mechanical properties of the alloy at the peak point of tensile strength and yield strength at 470 °C for different solution times.

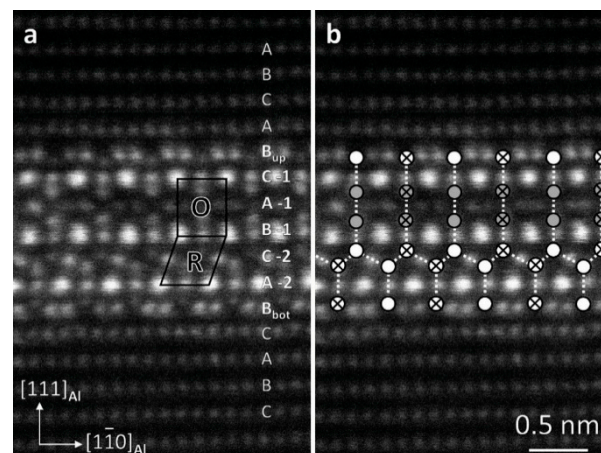


Figure 10. Lattice and crystal structure of 7xxx series aluminum alloy under haddf stem (a) STEM image of the η precipitate showing the continuity of stacking of the fcc aluminium lattice. (b) Overlay of the structure's skeleton made up from the major ligands. Adapted with permission from ref. [58]. 2020 Bendo et al.

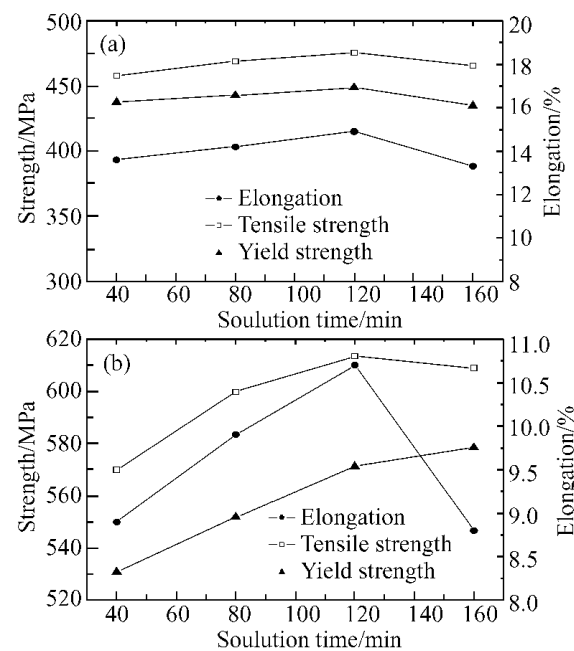


Figure 11. Change of tensile properties of studied alloy with solution time at 470 °C (a) solution (b) solution+T6. Adapted with permission from ref. [64]. 2007 Dai et al.

When the second phase is uniformly distributed in the matrix with fine dispersed particles, the precipitation strengthening or aging strengthening (dislocation cutting through the second phase mechanism) occurs when the second phase precipitates and produces a strengthening phase through the aging treatment of the supersaturated solid solution. If the second phase particles are strengthened by powder metallurgy, it is called dispersion strengthening [61,65]. The elements of the material composition affect the strength of the second phase particles, grain boundaries, grain size and orientation, grain boundaries and separation, and residual stress in the material. The formation of the second phase particles belongs to the diffusion-type phase transformation. When the dislocation meets the metastable precipitates such as η' (MgZn_2) phase, η_p ($\text{Al}_2\text{Mg}_2\text{Zn}_8$) phase, S' (Al_2CuMg) phase, β' (Al_8Mg_5) phase and T' ($\text{Al}_2\text{Mg}_2\text{Zn}_3$) in 7xxx series aluminum alloy, the dislocation will cut through the above metastable precipitates and deform with the matrix at the same time. The strength of the alloy is improved by increasing the interface energy between the second phase particles and the interface. When the dislocation meets the precipitated phase η with larger steady-state size, it is incoherent with the matrix. The dislocation will be subjected to the second-phase particles to make the dislocation line bend larger and form the second-phase particle dislocation ring. Other dislocations bypass the second-phase particles. The effect of the bypass mechanism on strengthening is enhanced with the increase in particles and the decrease in the size [62].

Kai Huang et al. [66] found that when Sc content was up to 0.25%, the grain dispersion strengthening refinement effect was effective, the particle size was more uniform, and the secondary dendrite spacing decreased. When the amount added was more than 0.30%, no grain refinement effect was observed, as shown in Figure 12.

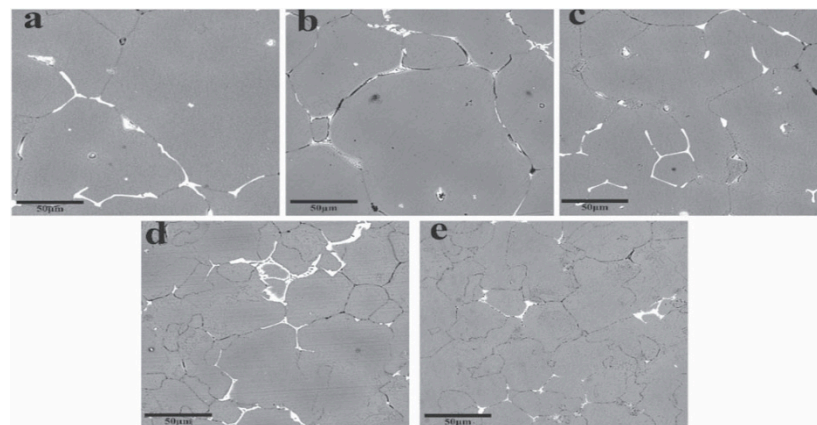


Figure 12. SEM images of 7055 as-cast alloys (a) Al-Y-0Sc, (b) Al-Y-0.2Sc, (c) Al-Y-0.25Sc, (d) Al-Y-0.3Sc, (e) Al-Y-0.35Sc. Adapted with permission from ref. [66]. 2021 Huang et al.

Figure 13 shows the high density $\text{Al}(\text{Sc}_x\text{Y}_y)$ particles in Al-0.25Y-0.25Sc alloy grains, some of which are located in the dislocation position near GBs. The precipitates first precipitate and grow at GBs, and then transform into a stable phase by absorbing the solute atoms around the particles [67]. The second phase particles of $\text{Al}_3(\text{Sc}_x\text{Y}_y)$ can prevent the movement of substructure and dislocation, and as the alloy has the smallest particle size, its corrosion resistance is the best. Zhang et al. [68] found that the second phase particles could inhibit the precipitation and aggregation of $\theta\text{-CuAl}_2$ phase at GBs, which greatly reduced the corrosion sensitivity of the alloy. When the η' (MgZn_2) phase is transformed into η phase, the strength and plasticity of the alloy decrease instead. The η phase distributed at the grain boundary will cause the formation of PFZ. Dislocation and stress concentration can lead to the expansion of PFZ into cracks [69].

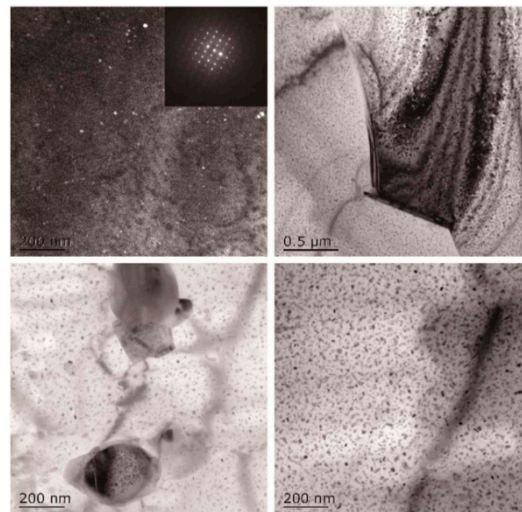


Figure 13. TEM topographic images of Al-0.25Y-0.25Sc alloy after aging. Adapted with permission from ref. [67]. 2018 Yan et al.

Both grain-boundary strengthening and processing-strengthening strengthen the material by changing the grain size. The prominent role of melting, and grain refinement, in improving the mechanical properties of aluminum products are two key issues [70]. The most obvious improvement in grain refinement is the increase in strength at room temperature, which can be explained theoretically by the Hall–Petch formula. In the polycrystalline, the yield strength is transferred from the grain with prior plastic deformation to the adjacent grain with slip. This transfer is reflected in the stress concentration generated by the dislocation accumulation group near the grain boundary of the slip grain. When the applied stress and other conditions reach a certain value, the number of dislocations is proportional to the distance between the obstacle causing the accumulation and the dislocation source at the grain boundary. Therefore, the larger the grain is, the larger is the distance, the larger the number of dislocations, and the greater is the stress concentration. The opportunity for plastic deformation is much larger than with small grains. This is why ductility increases with grain coarsening and decreases with grain size decreasing [62,70]. Compared with the second phase strengthening and deformation hardening, the grain boundary strengthening can improve the strength, toughness and ductility, and reduce the defects such as separation and porosity of castings [71].

3.2.2. Strengthening and Toughening Method

The strengthening and toughening methods of 7xxx series aluminum alloys should not be limited to the simple design of the alloy composition in the “stir-frying style”. We should focus more on the microstructure of the precipitates and the microstructure improvement methods after heat treatment. More attention should be paid to how to eliminate S (Al_2CuMg) phase, θ (CuAl_2) phase and T ($\text{Al}_2\text{Mg}_2\text{Zn}_3$) phase, and how to control the content of Mg/Zn to reduce the incoherent precipitation caused by η' (MgZn_2) phase. The addition of Zr and Sc atoms can form the dispersed $\text{Al}_3(\text{Sc,Zr})$ particles that are coherent with the matrix, which can refine the grains and inhibit the recrystallization of the grain boundary. However, the transformation of $\text{Al}_3(\text{Sc,Zr})$ particles from coherent to non-coherent should be avoided during the migration of the grain boundary. The non-coherent second phase particles will make the stress-corrosion resistance of the material worse and the quenching sensitivity higher.

Furthermore, the method of strengthening and toughening aluminum alloy should be combined with theoretical simulation and experiment, focusing on the optimization of 7xxx series aluminum alloy deformation processing and heat treatment on the microstructure and stress changes. Alistair Garne et al. [72] found the quenching of 7050 and 7085 aluminum alloy η phase nucleation simulation, shown in Figure 14, and obtained the

quenching process between the two alloys' q-GBPs (quenching state) and a-GBPs (aging state) composition in the volume composition difference. Menzemer et al. [73] studied the fracture surface morphology of 7085 at various temperatures, as shown in Figure 15. The alloy quenched in cold water showed the main intergranular fracture characteristics. When quenching in oil medium, the fracture surface transforms into a combination of transverse and intergranular fracture. It can be seen that heat treatment methods such as hierarchical solid solution and aging can promote the dispersion and homogenization of η' phase, and hinder the coarsening of PFZ region, thereby improving the strength and toughness of the alloy [74].

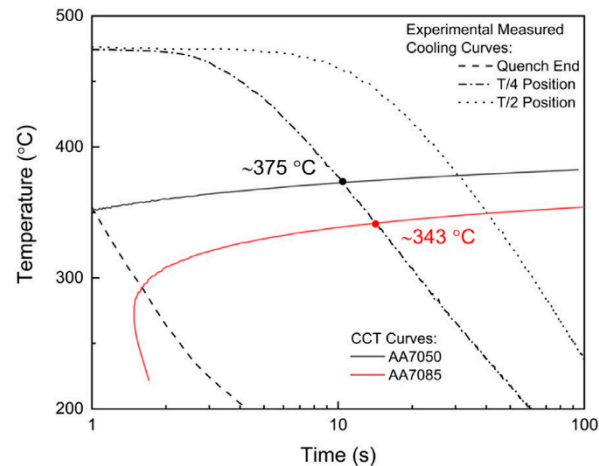


Figure 14. CCT curves for nucleation of η -phase Q-GBPs in AA7050 and AA7085. Adapted with permission from ref. [72]. 2021 Garner et al.

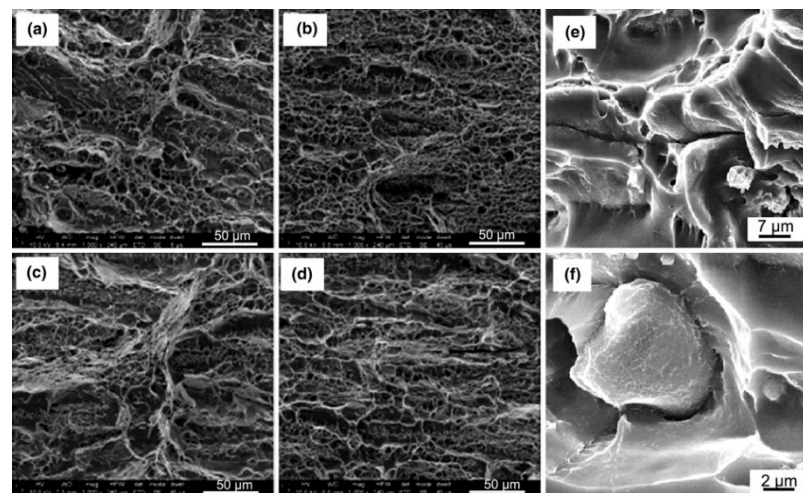


Figure 15. Fracture surface morphologies of AA7085 Al alloy under conditions of T6 (a), T74 (b), RRA (c), and HLA (d), temper conditions; high magnification images of fracture surface of AA7085 Al alloy show the cracking along the grain boundary triple points, dimples, and voids (e), cracking around coarse intermetallic particles (f). Adapted with permission from ref. [73]. 2010 Menzemer et al.

3.2.3. First-Principle Calculation of Precipitation Strengthening Phase

The first principle is based on the density functional theory (DFT), using the relativistic corrected projection augmented wave (PAW) method to describe the virtual element ratio; the crystal structure of the precipitated phase can be calculated, and the stability of the crystal structure can be judged. Liu et al. [75] calculated the interface energy of Al/ Al_3Sc , Al/ Al_3Er and $\text{Al}_3\text{Sc}/\text{Al}_3\text{Er}$ in Al-Sc-Er alloy in three directions, based on the PBE function in VASP software. It was found that the interface structure of (100) surface was the best, and

the interface energy of Al/Al₃Er was the largest, as shown in Figure 16. The L₁₂-Al₃Sc_xEr_{1-x} precipitates mainly formed a core-shell structure, with Al₃Er as the core, and Al₃Sc as the shell.

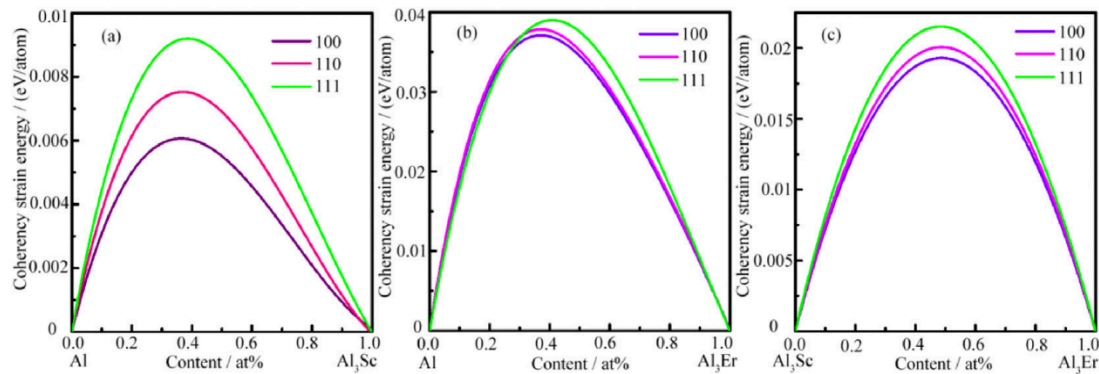


Figure 16. Coherency strain energies of (a) Al/Al₃Sc, (b) Al/Al₃Er, (c) Al₃Sc/Al₃Er on (100), (110), (111) interface planes. Adapted with permission from ref. [75]. 2021 Liu et al.

Dong et al. [76] discussed the effect of doping elements (M) on the structural stability and mechanical properties of Al₃Sc doped with Zr, Ti, Y and Li, as shown in Figure 16. The calculation shows that the structural stability, elastic properties and anisotropy of Al₂₄Sc₆Zr₂ and Al₂₄Sc₆Ti₂ are superior. Sun et al. [77] calculated that the point defects of L₁₂-Al₃Sc were mainly Al vacancies and Sc antisite defects on the Al sublattice, as shown in Figure 17. Various mechanical properties of the material were calculated by the first principle method and the mechanical equation, which was convenient for the study of the total amount and proportion of the main alloy elements of the aluminum alloy, and was a new direction in the field of material design [61].

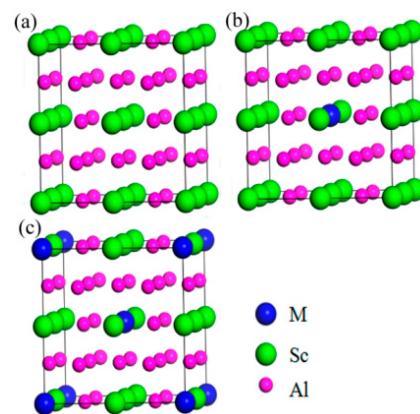


Figure 17. Structures of Al₃Sc cell structure of alloy elements (M = Sc, Zr, Ti, Y, Li) doped with different doping concentrations: (a) 2 × 2 × 2 supercell; doped with the alloying element (M = Sc, Zr, Ti, Y, Li) at different doping concentrations, (b) 3.125%, and (c) 6.25%. Blue, green, and pink balls represent (M = Zr/Ti/Y/Li), Sc, and Al atoms, accordingly. Adapted with permission from ref. [77]. 2013 Sun et al.

4. Preparation Method of 7xxx Series Aluminum Alloy

With regards to 7xxx series aluminum alloy, Fe and Si elements are considered as a natural impurities; solid solubility at room temperature is extremely low for insoluble intermetallic particles; insoluble intermetallic particles only through deformation and heat treatment alter the morphology, crystal type and composition [78]. All coarse intermetallic particles are principal formed in the process of direct cold casting. The non-uniformity of alloy is the difficulty and critical in the design and preparation of large-scale materials.

For avoiding performance loss in the manufacturing process. The integrated molding of materials is also a development trend. The sophisticated formation mechanism of macroscopic, microscopic and multi-scale structures involved in the relationship of alloy composition-process-structure-performance is the main reason for determining the properties of materials [79,80]. Figure 18 shows the process-microstructure-performance relationship of 7xxx series aluminum alloy.

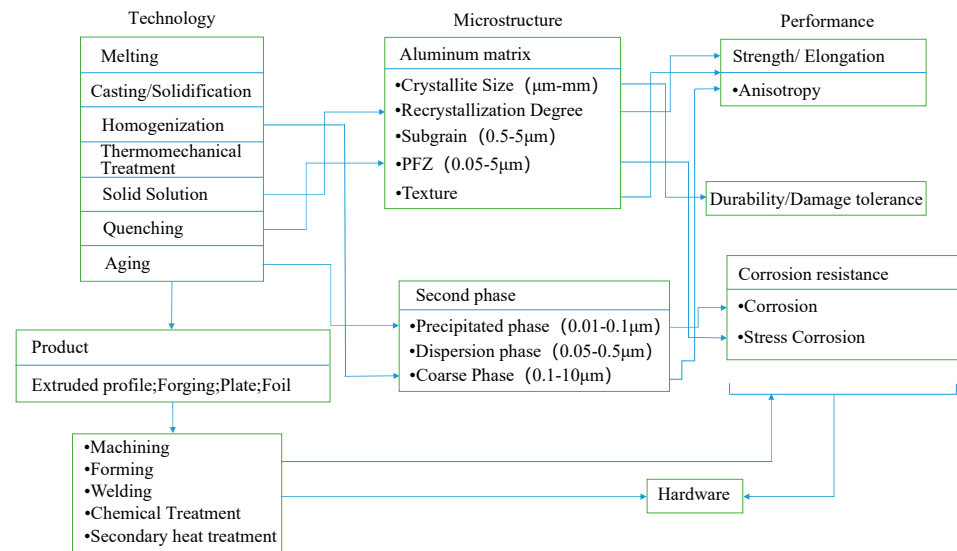


Figure 18. Technology microstructure performance relationship of 7xxx series aluminum alloy. Adapted with permission from ref. [79]. 2019 Deng and Zhang.

4.1. Casting Processes

The commonly used casting process for 7xxx series aluminum alloy is assigned to semi-continuous casting and squeeze casting. The casting structure mainly consists of primary α -Al, $MgZn_2$, $AlCuMg$, Al_2Cu and other second phases. With the decrease in pouring temperature, the primary α -Al dendrites in the slurry gradually decrease, and the near-isometric primary phase gradually increases. The grain size decreases, and the average roundness increases. In the solidification process of casting, the equilibrium or metastable phase formed by liquid-solid eutectic reaction occurs [80–82]. Bai [83] measured the chemical-mechanical properties of semi-solid 7050 alloy by in situ solidification method. It was found that the tensile strength and plasticity of the alloy initially decreased sharply with the decrease in solid fraction, which was due to the sharp decrease in the degree of intercrystalline polymerization of the semi-solid alloy with the increase in liquid phase. The tensile strength of the alloy decreased only slightly while the plasticity increased significantly. Thus, in the casting process it is most important to avoid macro segregation, cracks and other defects.

4.2. Multistage Homogenization Heat Treatment of Ingot

Firstly, 7xxx series aluminum alloy has a high degree of alloying, and the dendrite segregation of chemical composition in the ingot is especially obvious. The ingot of this alloy must be homogenized in the processing to eliminate the dendrite segregation of alloying elements and low melting point non-equilibrium eutectic phase, and reduce the heterogeneity of composition and structure. In practical engineering, the melting point of the non-equilibrium eutectic phase is usually measured by differential thermal analysis (DTA) or the differential scanning calorimetry (DSC) curve, and the melting temperature below the melting temperature of non-equilibrium eutectic phase is selected as the starting temperature of homogenization [84].

Secondly, another purpose of homogenization heat treatment is to regulate the behavior of high melting point precipitates of microalloying elements. The homogenization

temperature of 7xxx alloy ingots is usually below 470 °C, because 480 °C is considered to be the over-burning temperature of 7xxx series aluminum alloy [79,85], at which time a large amount of residual components may still exist. In the case of large and thick aluminum alloy sheets or shaped ingots, it is difficult to synchronize the lifting and cooling rates, so it cannot be optimized only by single-stage homogenization. Wang et al. [86] found that the highest temperature of two-stage homogenization treatment of 7B04 aluminum alloy can reach 500 °C. The most appropriate homogenization heat treatment process is heating at 10 °C/h to 470 °C for 64 h, and then heating at 1 °C/h to 500 °C for 10 h. By comparing the non-equilibrium solidification components of 7B04 aluminum alloy ingot after ultra-high temperature homogenization at 500 °C, they were completely dissolved in the alloy matrix; the hot rolling plasticity is much better than that of the traditional hot rolling plasticity after homogenization at 470 °C.

The morphologies of 7055 and 7055-0.25Sc ingots after homogenization are shown in Figure 19 [87]. The energy dispersive X-ray spectroscopy (EDS) spectrum of particle A, Figure 12a shows that the particle is in the θ phase. The EDS results measured by particle B in Figure 19b correspond to w (AlCuSc) phase. In the Al-Cu-Sc system with high copper content, Sc atoms diffuse to the θ phase, resulting in the transformation of θ phase into w phase during homogenization [88,89]. When the total mass fraction of Sc and Zr exceeds 0.45 wt%, w phase, primary Al_3 (Sc, Zr) phase and refined grains are insufficient, and the mechanical properties of 7055-xZrSc rolled plate treated with T6 deteriorate, thus 7055-0.25Sc rolled plate shows the optimal mechanical properties in the prepared alloy.

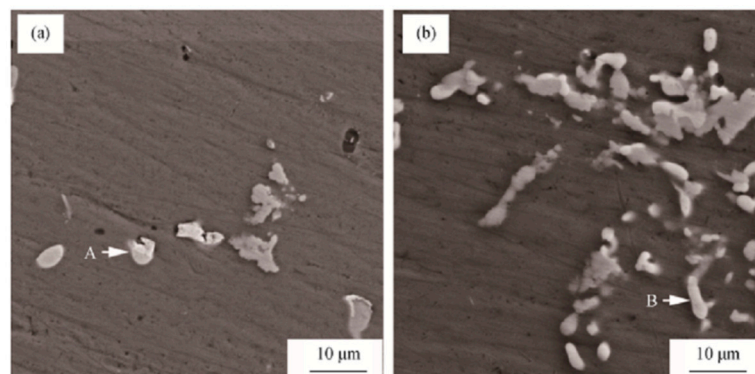


Figure 19. SEM images of homogenized ingots: (a) 7055; (b) 7055-0.25Sc. Adapted with permission from ref. [87]. 2019 Liu et al.

4.3. Forming Process

The conventional deformation processes of 7xxx alloy, including equal channel angular pressing (ECAP), asynchronous rolling (ASR), high pressure torsion (HPT), accumulative roll-over (ARB) and reciprocating extrusion (CEC), include rolling, extrusion, and forging [79]. Additive manufacturing is a technology of manufacturing solid parts by the gradual build-up of materials. Powder metallurgy (PM), and severe plastic deformation (SPD) are well-known technological solutions used to achieve properties [90,91]. In recent years, some high energy beam welding, including electron beam welding (EBW) and laser welding (LBW), and friction stir welding (FSW) have been applied to weld 7xxx aluminum alloy. Friction stir welding (FSW) is a solid-phase joining technology, rapidly developed in recent decades. The biggest difference from other welding processes mentioned above is that FSW has a low welding temperature, and no welding pool is generated during welding [92].

Whether using a traditional forming process or a new additive manufacturing process, what is required is to research the elimination of manufacturing defects through the deformation process, and the production of ultra-fine grain microstructure resulting from work hardening and fine-grain strengthening to improve the mechanical properties of materials

and increase the precipitation density of η' phase, which is also a far-reaching method used for strengthening alloys in industry.

Asynchronous rolling can be called snake rolling according to the process characteristics. Asynchronous rolling introduces shear strain and increases the deformation of the core plate, which can effectively solve the serious uneven strain distribution of aluminum alloy plate in the symmetric rolling process. Xu et al. [93] found that the strength performance of the alloy plate increased with the increase in the speed ratio, and the elongation and fracture toughness decreased. When the speed ratio is the same, with the increase in offset, the strength of serpentine rolled sheet decreases, and the elongation and fracture toughness increases significantly. In the condition where offset is 10 mm and speed ratio is 1:1, the crack unit nucleation energy of the serpentine rolled sample increases by 14~36%. Xia [94] simulated the asynchronous rolling of magnesium alloy sheets. The results show that under the condition of the same total deformation, the multi-pass asynchronous rolling with small speed ratio cannot only effectively obtain large shear strain accumulation, but also the distribution of equivalent strain is more uniform than that of large speed ratio rolling, and the multi-pass alternating asynchronous rolling can significantly improve the high uniformity of thick plates.

Figure 20 shows the schematic diagram of snake rolling [95]. As shown in the figure, the lower roller moves a distance (Δ) horizontally relative to the upper roller, and the peripheral speed ratio (v_u/v_l) between the upper and lower rollers can be adjusted by altering the speed ratio (ω_u/ω_l) or diameter (d_u/d_l). Extensive studies have shown that the snake rolling method can, not only refine the grain, but also change the crystal structure [96–98].

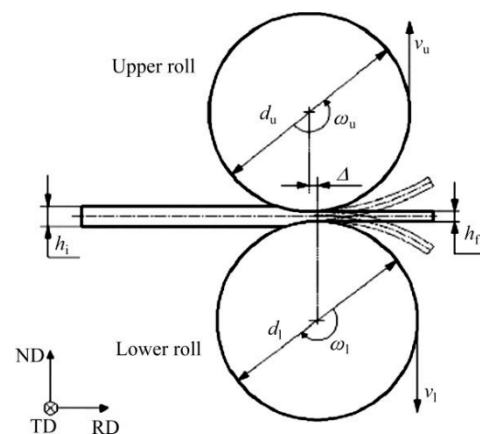


Figure 20. Schematic diagram of snake rolling. Adapted with permission from ref. [95]. 2016 Li et al.

4.4. Heat Treatment Method

The purpose of heat treatment is to adjust the method suitable for the material properties according to grain size, solute atoms, GBPs and microstructure of precipitates, mainly including solid solution treatment and artificial aging treatment. Methods such as single-stage and multi-stage solution, peak aging, excessive aging, multi-stage aging and regression re-aging are widely applicable.

4.4.1. Solution Treatment

Solid solution treatment, known as quenching, is the basis of strengthening heat treatment (quenching and aging) of aluminum alloy strengthened by heat treatment [99]. Solid solution treatment is classified into single-stage solid solution treatment (SST), enhanced solid solution treatment (EST), high temperature pre-precipitation (HTPP) and multi-stage solid solution treatment (MST) [100–102]. The objective of solid solution is to dissolve the alloying elements into the aluminum matrix to achieve a well strengthening effect in the subsequent aging precipitation stage. The single-stage temperature and constant-

temperature multi-stage solid solution method can effectively alleviate the coarsening of alloy grains at high temperature. In multi-stage solution treatment (MST), the heating and holding process is divided into several stages from low temperature to high temperature, which can significantly improve the comprehensive performance of aluminum alloy. Feng et al. [100] used (470 °C,1h) + (480 °C,1h) two-stage solid solution treatment for 7A55 alloy to eliminate the non-equilibrium of the surface layer of 7A55 aluminum alloy thick plate η' . With high phase volume fraction, the heterogeneity of hardness and conductivity of 7A55 aluminum alloy thick plate can be improved. The commonly used solid solution process of 7xxx series aluminum alloy is [103,104] 450 °C/2 h + 460 °C/2 h + 470 °C/2 h + 480 °C/2 h. After water-cooled solid solution strengthening and 121 °C/12 h aging treatment, the alloy can obtain better mechanical properties, and the strength, hardness and plasticity become superior. Figure 21 [105] shows the second-phase distribution after different solid solution treatments. It can be seen that the solution treatment will significantly affect the grain size of the alloy and the solid solution degree of the solute atoms, thus changing the precipitation kinetics of the alloy in the subsequent aging process, and the number and density of the aging precipitates will ultimately determine the overall performance of the alloy.

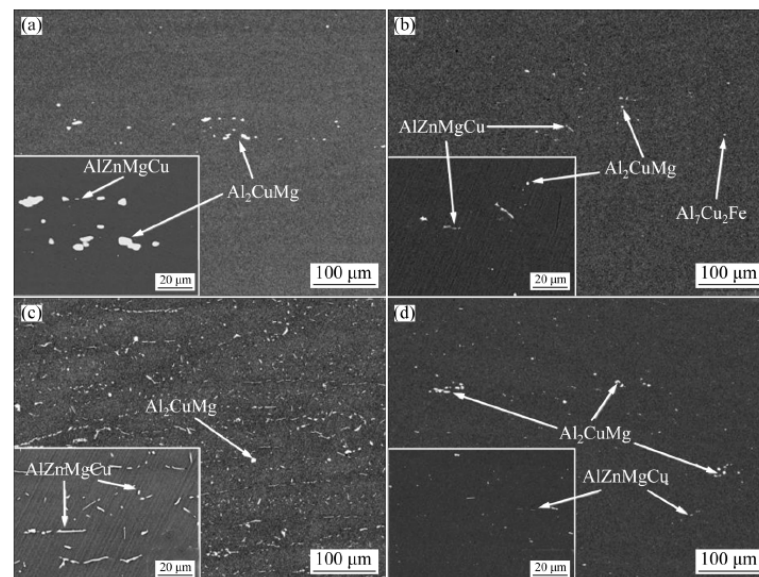


Figure 21. Second-phase distribution after different solid solution treatments in 7055: (a) SST; (b) EST; (c) HTPP; (d) MST. Adapted with permission from ref. [105]. 2021 Zhang et al.

4.4.2. Aging Treatment

The traditional 7xxx series aluminum alloy has high strength after peak aging (T6) treatment, but its SCC performance is low. Although over-aging treatment can greatly improve the corrosion resistance of the alloy, the strength loss is large. In order to solve this problem, regression re-aging (RRA) is introduced to balance the properties of materials [106,107]. Zheng et al. [108] improved T6176 intermittent aging system for 7475 aluminum alloy thick plate, and obtained the strength equivalent of T6 state and the local corrosion performance better than that of T73. Aging is a non-isothermal process. Ding [109] identified the effects of T6, four-stage aging, three-stage aging and T74 on thermal stability by tensile test, transmission electron microscopy (TEM) and atomic probe tomography (APT). The results showed that the tensile strength of the four-stage aging sample decreased by only 5.05% after thermal exposure at 120 °C for 500 h. For the regression re-aging (RRA) treatment with stricter control of heat treatment time, the temperature of this process is high, and the precipitated phase will experience multiple reactions of dissolution, nucleation, growth and coarsening, respectively, or simultaneously in different regression temperature ranges. The hardness of 7xxx series aluminum alloy is higher than that of T651 (HV180) when the

RRA heat treatment is carried out at a relatively low temperature (180 °C) and with a short degradation period. However, with the increase in temperature, the hardness decreases with the increase in the degradation period. After RRA treatment at 180 °C for 4 min, the hardness is the highest. The hardness of 7xxx series aluminum alloy is higher than that of T651 (HV180) when RRA heat treatment is carried out at a relatively low temperature (180 °C) and with a short degradation period, but with the increase in temperature, the hardness decreases with the increase in degradation period, and the hardness reaches the highest after RRA heat treatment at 180 °C for 4 min [79,110]. Liao [111] carried out different combinations of pre-aging, regression treatment and re-aging systems on 7055, and obtained the optimum RRA system for actual production in the factory, which is 120 °C/24 h + 175 °C/1.5 h + 120 °C/24 h, in which the heating rate is 35 °C/h, and the cooling method is air cooling. The results show that the pre-aging temperature has more effect on the size of the precipitated phase than the re-aging temperature. After RRA treatment [112], the material will be over-aged. During the re-aging process, a new precipitate occurs in the η' phase, while the coarse η' precipitate grows and transforms into the η phase. It shows the regression stage undergoes heating, heat preservation, cooling and other processes, and there are many kinds of precipitates in the crystal, and the evolution law is sophisticated. However, the precipitation is a single type of equilibrium. Therefore, for the RRA treatment, the grain boundary precipitates can be selected as the object, and the non-isothermal regression kinetic model can be established to guide the precise regulation of aging process parameters.

5. Challenges and Conclusions

The biggest challenge for aluminum alloy today is that in order to greatly improve the corrosion resistance of the alloy, the strength loss is large. Both cannot be improved at the same time. Furthermore, due to the low melting point of aluminum alloy, its high temperature properties need to be improved. More attention should be paid to how to simultaneously improve the corrosion resistance and strength at the same time. Additive manufacturing of aluminum alloy, which has the characteristics of uniform chemical composition, high density, open forming environment, unlimited size of forming parts and high forming rate, is also the focus of future research. The optimization of alloy composition design and improvement of heat treatment method are the specific means to improve the comprehensive performance of 7xxx series aluminum alloy. The break-through of aluminum alloy composition design-microstructure characterization theory and research method promotes the development process of high strength aluminum alloy. Based on the research content, the research directions and methods of 7xxx series aluminum alloys in the future are determined as follows:

- To investigate the total amount and proportion of the main alloy elements and the action law of microalloying elements, Thermo-Calc, VASP, Factsage, Materials Studio and other software can be employed to integrate theoretical calculation, simulation and experiment. The research and development, performance improvement and product development period of alloys can be considerably shortened, and the efficiency can be improved immensely.
- Under the guidance of the calculation results of the first-principles theory, the microstructure-property characterization method of aluminum alloy was continuously improved according to the relationship among alloy composition, process, microstructure and property. The new principle and characterization method of the process-microstructure-property correlation of materials was developed to explore the characteristic microstructure 7xxx series aluminum alloy materials with high static strength, high strength, heat resistance, high toughness, damage resistance, low density, low quenching sensitivity, and high comprehensive performance, at the cutting edge.
- The η' Phase is the only strengthening phase in the alloy, in order to increase the volume fraction of η' precipitates and modify strength, rare earth elements should be added to the alloy, while controlling the Mg/Zn mass ratio in the range of 5:2–7:1

can refine the precipitates and improve the strength of the alloy and keep the alloy corrosion resistant.

- Sc rare earth element is currently the most significant alloying element, $\text{Al}_3(\text{Sc,Zr})$ particles with L1_2 structure precipitated at any time into coherent $\text{Al}_3(\text{Sc,Zr})$ particles with D0_{23} structure can effectively hinder recrystallization, inhibit grain growth, and improve the mechanical properties of the alloy. Er and Sc rare earth elements are relatively low, and the eutectic point composition of Sc is the lowest, $w(\text{Sc})\% \approx 0.3\%$, $w(\text{Er}) \approx 1.0\%$. Therefore, it can be perceived that the properties of 7xxx series aluminum alloy with Sc addition will be remarkably improved. Er is much cheaper than Sc; consequently, Er is a potential rare earth element to replace Sc.
- The width, GBPs sum, distribution and continuity of the average PFZ determine the overall performance of the material; the purpose of different homogenization, multi-stage aging and RRA heat treatment is to adjust the method suitably to achieve material properties, according to grain size, solute atoms, GBPs and microstructure of precipitates.
- Although the heat treatment process of 7xxx series aluminum alloy requires controlling time lapses in the process of heating, holding and cooling, and there are many species precipitates in the crystal and the evolution mechanism is heterogeneous, the precipitated strengthening phase is a single type of equilibrium η' phase. Therefore, for the heat treatment process, the grain boundary precipitate can be selected as the object, and the non-isothermal regression kinetic model was established to guide the accurate regulation of aging process parameters. More attention should be paid to how to increase the volume fraction of η' precipitates and modify the comprehensive performance of the material by the regression re-aging method.
- Asynchronous rolling introduces shear strain and increases the deformation of the core plate, which can effectively solve the serious uneven strain distribution of aluminum alloy plate in the symmetric rolling process. The snake rolling method can not only refine the grain, but also change the crystal structure, therefore, it can be popularized for use.

Author Contributions: Conceptualization, investigation, writing—original draft preparation, Y.D.; data treatment, writing—review and editing, L.Y.; data treatment, J.H. All authors have read and agreed to the published version of the manuscript.

Funding: This research was funded by National Natural Science Foundation of China (Grant No. 51764043); Scientific and Technological Program of Innovation and Guidance of Inner Mongolia (Grant No. KCBJ2018017); Inner Mongolia Youth Talent Program of Science and Technology (NJYT-20-A16); Inner Mongolia Natural Science and Technology (Grant No. 2020MS05061).

Institutional Review Board Statement: Not applicable.

Informed Consent Statement: Informed consent was obtained from all subjects involved in the study.

Data Availability Statement: Not applicable.

Conflicts of Interest: The authors declare no conflict of interest.

References

1. Azarniya, A.; Abolfazl, T.; Karimi, T.; Kourosh, K. Recent advances in ageing of 7xxx series aluminum alloys: A physical metallurgy perspective. *J. Alloys Compd.* **2019**, *781*, 945–983. [[CrossRef](#)]
2. Wu, H.; Wen, S.P.; Lu, J.T.; Mi, Z.P.; Zeng, X.L.; Huang, H.; Nie, Z.R. Microstructural evolution of new type Al-Zn-Mg-Cu alloy with Er and Zr additions during homogenization. *Trans. Nonferr. Met. Soc. China* **2017**, *7*, 1476–1482. [[CrossRef](#)]
3. Zhou, B.; Liu, B.; Zhang, S.G. The advancement of 7xxx series aluminum alloys for aircraft structures: A review. *Metals* **2021**, *11*, 718. [[CrossRef](#)]
4. Imran, M.; Khan, A.A. Characterization of Al-7075 metal matrix composites: A review. *J. Mater. Res. Technol.* **2019**, *8*, 3347–3356. [[CrossRef](#)]
5. Wen, K.; Xiong, B.Q.; Zhang, Y.A.; Wang, G.J.; Li, X.W.; Li, Z.H.; Huang, S.H.; Liu, H.W. Microstructure Evolution of a High Zinc Containing Al-Zn-Mg-Cu Alloy during Homogenization. *Rare Met. Mat Eng.* **2017**, *4*, 928–934.

6. Prabhu, T.R. An overview of high-performance aircraft structural Al alloy-AA7085. *Acta Met. Sin.* **2015**, *28*, 909–921. [[CrossRef](#)]
7. Li, L.; Dong, L.; Wang, H.D.; Zhou, Y.X.; Gao, C. Research progress on corrosion fatigue of aerospace aluminum alloy. *Surf. Technol.* **2021**, *7*, 106–118.
8. Umamaheshwerao, A.C.; Vasu, M.; Govindaraju, K.V.; SaiSrinadh, K. Stress corrosion cracking behaviour of 7xxx series aluminum alloys: A literature review. *Trans. Nonferr. Met. Soc. China* **2016**, *26*, 1447–1471.
9. Wagner, J.A.; Shenoy, R.N. The effect of copper, chromium, and zirconium on the microstructure and mechanical properties of Al-Zn-Mg-Cu alloy. *Met. Trans. A* **1991**, *22*, 2809. [[CrossRef](#)]
10. Yuan, S.; Jia, L.N.; Zhang, H. Effects of Er on the microstructure and eutectic phase morphology of directionally solidified Al-Zn-Mg-Cu-Zr alloys. *Rare Met. Mater. Eng.* **2021**, *50*, 3477–3484.
11. Pang, X.Z. Research on the Effect of Alloying on Some Important Phases, Interfaces and Microstructure Evolution and Performance of Al-Zn-Mg-Cu Alloy. Ph.D. Thesis, South China University of Technology, Guangzhou, China, 2017.
12. Li, H.; Tang, K.; Wang, H.; Wang, K.S.; Li, Y.K.; Wu, Y.C. Precipitation behavior of Al-Zn-Mg-Cu-Sc-Zr alloy during homogenization process. *Chin. J. Nonferr. Met.* **2021**, *31*, 2403–2411.
13. Lee, S.H.; Jung, J.G.; Bail, S.I.; Seidman, D.N.; Kim, M.S.; Lee, Y.K.; Euh, K.J. Precipitation strengthening in naturally aged Al-Zn-Mg-Cu alloy. *Mater. Sci. Eng. A* **2021**, *803*, 140719. [[CrossRef](#)]
14. Senkov, O.N.; Bhat, R.B.; Senkova, S.V.; Schloz, J.D. Microstructure and properties of cast ingots of Al-Zn-Mg-Cu alloys modified with Sc and Zr. *Mater. Trans. A* **2005**, *36*, 2115–2126. [[CrossRef](#)]
15. Xu, D.; Li, Z.H.; Wang, G.J.; Li, X.W.; Lv, X.Y.; Zhang, Y.A.; Fan, Y.Q.; Xiong, B.Q. Phase transformation and microstructure evolution of an ultra-high strength Al-Zn-Mg-Cu alloy during homogenization. *Mater. Charact.* **2017**, *131*, 285–297. [[CrossRef](#)]
16. Xia, P.; Wang, S.C.; Huang, H.L.; Zhou, N.; Song, D.F.; Jia, Y.W. Effect of Sc and Zr additions on recrystallization behavior and intergranular corrosion resistance of Al-Zn-Mg-Cu alloys. *Materials* **2021**, *14*, 5516. [[CrossRef](#)]
17. Gu, D.D.; Zhang, H.; Liu, G.; Yang, B.Q. Process optimization of additive manufactured sandwich panel structure using rare earth element modified high-performance Al alloy. *Acta Aeronaut. Astronaut. Sin.* **2021**, *10*, 454–466.
18. Xu, X.F.; Zhao, Y.G.; Zhang, M.; Ning, Y.H.; Wang, X.D. Effect of extrusion ratio on the microstructure and mechanical properties in an Al-Cu-Mg-Ag alloy. *J. Wuhan Univ. Technol.* **2018**, *33*, 710–714. [[CrossRef](#)]
19. Zhang, X.L.; Chen, S.Y.; Zhou, L.; Fan, S.M.; Chen, K.H. Effect of composition on quenching sensitivity and microstructures-properties of super-strength Al-Zn-Mg-Cu aluminum alloys. *Rare Met.* **2019**, *43*, 561–570.
20. Wang, Y.C.; Cao, L.F.; Wu, X.D.; Zou, Y.; Huang, G.J. Research progress on microstructure and properties of 7xxx series aluminum alloys for oil drill pipes. *Mater. Rev.* **2019**, *33*, 1190–1197.
21. Li, Y. Effect of Alloy Elements on Microstructure and Hot Tearing Susceptibility in Direct-Chill Casting of 7xxx Series Aluminum Alloys. Ph.D. Thesis, University of Science and Technology Beijing, Beijing, China, 2019.
22. Dai, X.Y.; Li, N.; Xiong, L. Research progress of hardenability of Al-Cu-Mg-Ag alloys. *Mater. Rev.* **2015**, *29*, 75–80.
23. Zhao, Q.; Wang, S.X. *Selection and Design of Aluminum Alloy*, 1st ed.; Chemical Industry Press: Beijing, China, 2017; pp. 34–35.
24. Fang, H.C.; Yang, H.L.; Zhu, J.M.; Xiao, P.; Chen, Z.; Liu, T. Effect of minor Cr, Mn, Zr or Ti on recrystallization, secondary phases and fracture behaviour of Al-Zn-Mg-Cu-Yb Alloys. *Rare Met. Mater. Eng.* **2020**, *49*, 797–810.
25. Pan, Y.L. Study on Compositional Design, Microstructure and Properties of Novel High-Strength Al-Zn-Mg-Cu Aluminum Alloy with Good Weldability and Corrosion Resistance. Ph.D. Thesis, University of Science and Technology Beijing, Beijing, China, 2021.
26. Gao, Y.H.; Liu, G.; Sun, J. Recent progress in high-temperature resistant aluminum-based alloys: Microstructural design and precipitation strategy. *Acta Met. Sin.* **2021**, *57*, 129–149.
27. Bhuiyan, M.S.; Toda, H.; Uesugi, K.; Takeuchi, A.; Watanabe, Y. Damage micromechanisms in high Mn and Zn content 7xxx series aluminum alloys. *Mater. Sci. Eng. A* **2020**, *793*, 139423. [[CrossRef](#)]
28. Valeev, I.S.; Barykin, N.P.; Trifonov, V.G.; Valeeva, A.K. Effect of powerful current pulses on the structure and mechanical properties of the aluminum alloy Al-6%Mg-0.6%Mn. *J. Mater. Eng. Perform.* **2014**, *14*, 236–240. [[CrossRef](#)]
29. Wang, Z.P.; Wang, M.L.; Li, Y.G.; Xiao, H.Y.; Chen, H.; Geng, J.W.; Li, X.F.; Chen, D.; Wang, H.W. Effect of pretreatment on microstructural stability and mechanical property in a spray formed Al-Zn-Mg-Cu alloy. *Mater. Des.* **2021**, *203*, 109618. [[CrossRef](#)]
30. Hu, G.Y.; Zhu, C.Z.; Xu, D.F.; Dong, P.X.; Chen, K.H. Effect of cerium on microstructure, mechanical properties and corrosion properties of Al-Zn-Mg alloy. *J. Rare Earth* **2021**, *39*, 208–216. [[CrossRef](#)]
31. Chai, W.R.; Chen, J.C.; Liu, S.D.; Ye, L.Y.; Lin, H.Q.; Zhang, X.M. Effect of minor Zr addition on exfoliation corrosion resistance of Al-Zn-Mg-Mn alloy sheet. *Chin. J. Mater. Res.* **2019**, *33*, 488–496.
32. Fang, H.C.; Chao, H.; Chen, K.H.; Zhang, Z. Microstructures fracture and localized corrosion behaviors of Al-Zn-Mg-Cu alloy with Zr, Yb and Cr additions. *Rare Met.* **2015**, *39*, 686–695.
33. Feng, C.; Shou, W.B.; Liu, H.Q.; Yi, D.Q.; Feng, Y.R. Microstructure and mechanical properties of high strength Al-Zn-Mg-Cu alloys used for oil drill pipes. *Trans. Nonferr. Met. Soc. China* **2015**, *25*, 3515–3522. [[CrossRef](#)]
34. Xu, X.F. Study on the Microstructure Evolution and Toughening-Strengthening in Al-Cu-Mg-(Ag)/Al-Zn-Mg-Cu-(Ag) Alloys. Ph.D. Thesis, Jilin University, Jilin, China, 2015.
35. Yu, C.; Chen, L.P.; Zhou, Q. Research progress in effects of rare earth elements on microstructure and properties of aluminum alloy. *Spec. Cast Nonferr. Alloy.* **2021**, *41*, 241–246.

36. Wang, D.W.; Fu, Y.D.; Li, T.; Cong, F.G. Role of rare earth elements in wrought aluminum alloys and their development trend. *Light Alloy. Fabr. Technol.* **2020**, *48*, 19–24.
37. Xiao, J.M.; Huo, M.Y. *Theoretical and Applied Researches on Rare Earths in China*, 1st ed.; Higher Education Press: Beijing, China, 1992; pp. 81–83.
38. Liu, G.H. *Rare Earth Materials and Application Technology*, 1st ed.; Chemical Industry Press: Beijing, China, 2005; pp. 151–152.
39. Liu, L.H.; Liu, L.F.; Cao, F.H.; Yang, T.; Yin, P.Z. Effect of Er element on impact deformation and failure behaviors of 7xxx series aluminum alloy. *Ordinance Mater. Sci. Eng.* **2020**, *43*, 125–130.
40. Huang, Y.C.; Zhang, C.C.; Ren, X.W.; Liu, Y.; Chen, S.Z.; Wang, Y.L. Existence form of trace Er in Al-Zn-Mg-Cu alloy and its “genetic effect”. *Rare Metal Mater. Eng.* **2019**, *48*, 2848–2856.
41. Li, Z.M.; Jiang, H.C.; Wang, Y.L.; Zhang, D.; Yan, D.S.; Rong, L.J. Effect of minor Sc addition on microstructure and stress corrosion cracking behavior of medium strength Al-Zn-Mg alloy. *J. Mater. Sci. Technol.* **2018**, *34*, 1172–1179. [[CrossRef](#)]
42. Liu, L. Sc and Zr Microalloying Effects and Microscopic Mechanisms in Al Alloys. Ph.D. Thesis, Harbin Institute of Technology, Harbin, China, 2020.
43. Xiao, Q.F.; Huang, J.W.; Jiang, Y.G.; Jiang, F.Q.; Wu, Y.F.; Xu, G.F. Effects of minor Sc and Zr additions on mechanical properties and microstructure evolution of Al-Zn-Mg-Cu alloys. *Trans. Nonferr. Met. Soc. China* **2020**, *30*, 1429–1438. [[CrossRef](#)]
44. Li, G.F.; Zhang, X.M.; Zhu, H.F. Effect of minor Er and Y additions to Al-Zn-Mg-Cu-Zr alloy on homogenizing behavior. *J. Aeronaut Mater.* **2010**, *30*, 1–6.
45. Chen, K.H.; Jian, S.S.; Zhou, L.; Chen, S.Y.; Huang, L.P. Effect of trace rare earth element Gd on microstructure and corrosion resistance of 7056 aluminum alloy. *J. Hunan Univ. Nat. Sci. Ed.* **2020**, *47*, 96–107.
46. Mei, F.Q.; Wang, S.H.; Fang, C.F.; Meng, L.G.; Jia, F.; Hao, H.; Zhang, X.G. Effect of Gd content on microstructures and mechanical properties of Al-Zn-Mg-Cu-Zr alloys. *Chin. J. Nonferr. Met.* **2012**, *22*, 2439–2447.
47. Rokhlin, L.L.; Dobatkina, T.V.; Bochvar, N.R. Investigation of phase equilibria in alloys of the Al-Zn-Mg-Cu-Zr-Sc system. *J. Alloys Compd.* **2004**, *367*, 10–16. [[CrossRef](#)]
48. Zhang, X.M.; Deng, Y.L. *China’s Strategic Emerging Industry-New Alloy Materials*, 1st ed.; China Railway Publishing House: Beijing, China, 2018; pp. 25–26.
49. Won, S.J.; So, H.K.; Leeseung, O.; Soong, J.K.; Kyou, H. Development of a high-strength Al-Zn-Mg-Cu-based alloy via multi-strengthening mechanisms. *Scr. Mater.* **2021**, *205*, 114216. [[CrossRef](#)]
50. Yu, X.W. Study on the Relationship between 3D Microstructure and Properties of Al-Zn-Mg-(Cu) Alloy During Pre-Deformation and Aging. Ph.D. Thesis, Hunan University, Hunan, China, 2020.
51. Priya, P.; Johnson, D.R.; Krane, M.J.M. Precipitation during cooling of 7xxx series aluminum alloys. *Comput. Mater. Sci.* **2017**, *139*, 273–284. [[CrossRef](#)]
52. Zhang, Y.; Li, H.P.; Kang, W.; Zhang, X.M. Aging microstructure evolution in high strength aluminum alloys and performance controlling. *Chin. J. Nonferr. Met.* **2017**, *27*, 1323–1336.
53. Yu, X.W.; Chen, J.H.; Ming, W.Q.; Yang, X.B.; Zhao, T.T.; Shen, R.H.; He, Y.T.; Wu, C.L. Revisiting the Hierarchical Microstructures of an Al-Zn-Mg Alloy fabricated by pre-deformation and aging. *Acta Met. Sin.* **2020**, *33*, 1518–1526. [[CrossRef](#)]
54. Bakhshi, R.; Farshidi, M.H.; Sajjadi, S.A. Strengthening of aluminium alloy 7005 through the imposition of severe plastic deformation supplemented by different ageing treatments. *Chin. J. Nonferr. Met.* **2021**, *31*, 2909–2921. [[CrossRef](#)]
55. Zang, J.X.; Dai, P.; Yang, Y.Q.; Liu, S.; Huang, B.; Ru, J.G.; Luo, X. Study on the Relationship between High Temperature Mechanical Properties and Precipitates Evolution of 7085 Al Alloy after Long Time Thermal Exposures. *Metals* **2021**, *11*, 1483. [[CrossRef](#)]
56. Khalfallah, A.; Raho, A.A.; Amzert, S.; Djemli, A. Precipitation kinetics of GP zones, metastable η' phase and equilibrium η phase in Al-5.46wt.%Zn-1.67wt.%Mg alloy. *Trans. Nonferr. Met. Soc. China* **2019**, *29*, 233–241. [[CrossRef](#)]
57. Berg, L.K.; Gjøønnes, J.; Hansen, V.; Li, X.Z.; Knutson-Wedel, M.; Waterloo, G.; Schryvers, D.; Wallenberg, L.R. GP-zones in Al-Zn-Mg alloys and their role in artificial aging. *Acta Mater.* **2001**, *49*, 3443–3451. [[CrossRef](#)]
58. Bendo, A.; Matsuda, K.; Nishimura, K.; Nunomura, N.; Tsuchiya, T.; Lee, S.; Marioara, C.D.; Tsuru, T.; Yamaguchi, M.; Shimizu, K.; et al. The possible transition mechanism for the meta-stable phase in the 7xxx aluminium. *Mater. Sci. Technol. Lond.* **2020**, *36*, 1621–1627. [[CrossRef](#)]
59. Chen, Y.X. Microstructure and Texture in the Surface Gradient Nanostructured Nickel and Aluminum Alloys. Ph.D. Thesis, Northwestern Polytechnical University, Xi’an, China, 2018.
60. Garbicz, D.; Leshchynsky, V.; Garcia-Junceda, A.; Swadzba, R.; Siwak, P.; Adamek, G.; Radwanski, K. Microstructure and mechanical properties of spark plasma sintered and severely deformed AA7075 alloy. *Metals* **2021**, *11*, 1433. [[CrossRef](#)]
61. Wang, Y.C.; Tong, X.; You, G.Q.; Cao, L.F. Research progress and prospects of the microstructures, properties, and forming techniques of Al-Li Alloy. *Rare Met. Mater. Eng.* **2021**, *50*, 1069–1083.
62. Cui, Z.Q.; Tan, Y.C. *Metallography and Heat Treatment*, 2nd ed.; Machinery Industry Press: Beijing, China, 2008; pp. 176–178.
63. Shu, W.X. Solidification Characteristics and Strengthening-Thoughening Mechanisms of 7xxx Al Alloys with Tailored Mg and Cu Elements. Ph.D. Thesis, University of Science and Technology Beijing, Beijing, China, 2015.
64. Dai, X.Y.; Xia, C.Q.; Liu, C.B.; Gu, Y. Effects of solution treatment and aging process on microstructure and mechanical properties of 7xxx aluminium alloy. *Trans. Mater. Heat Treat.* **2007**, *4*, 59–63.
65. Yu, H.Q. *Principle of Metal Plastic Forming*, 1st ed.; Machinery Industry Press: Beijing, China, 2018; pp. 12–13.

66. Huang, K.F.; Qin, Z.; Zhou, W.B.; Ren, Y.L.; Huang, L.; Xiang, J.; Tang, H.Q.; Zhu, Y.T.; Wei, Y.Z. Enhancement of strength mechanical and corrosion resistance of 7055 alloy with minor Sc and Y addition. *Mater. Res. Express* **2021**, *8*, 016524. [[CrossRef](#)]
67. Yan, Y.C.; Huang, B.; Li, W.J.; Qing, P.L.; He, B. Research progress of Al-Zn-Mg-Cu Ultra-high Strength aluminum alloy. *Mater. Rev.* **2018**, *32*, 358–364.
68. Zhang, X.G.; Mei, F.Q.; Zhang, H.Y.; Wang, S.H.; Fang, C.F.; Hao, H. Effects of Gd and Y additions on microstructure and properties of Al-Zn-Mg-Cu-Zr alloys. *Mater. Sci. Eng. A* **2012**, *552*, 230–235. [[CrossRef](#)]
69. Huang, L.P.; Chen, K.H.; Li, S. Influence of grain-boundary pre-precipitation and corrosion characteristics of inter-granular phases on corrosion behaviors of an Al-Zn-Mg-Cu alloy. *Mater. Sci. Eng. B* **2012**, *177*, 862–868. [[CrossRef](#)]
70. Guan, R.G.; Tie, D. A Review on Grain Refinement of Aluminum Alloys: Progresses, Challenges and Prospects. *Acta Met. Sin.* **2017**, *30*, 409–432. [[CrossRef](#)]
71. Charit, I.; Mishra, R. Effect of friction stir processed microstructure on tensile properties of an Al-Zn-Mg-Sc alloy upon subsequent aging heat treatment. *J. Mater. Sci. Technol.* **2018**, *34*, 214–218. [[CrossRef](#)]
72. Garner, A.; Euesden, R.; Yao, Y.; Aboura, Y.; Zhao, H.; Donoghue, J.; Curioni, M.; Gault, B.; Shanthraj, P.; Barrett, Z.; et al. Multiscale analysis of grain boundary microstructure in high strength 7xxx Al alloys. *Acta Mater.* **2021**, *202*, 190–210. [[CrossRef](#)]
73. Menzemer, C.C.; Lam, D.F.; Srivatsan, T.S. An investigation of strain concentration in high-strength Al-Zn-Mg-Cu alloy 7085 subjected to tensile deformation. *J. Mater. Eng. Perform.* **2010**, *5*, 705–713. [[CrossRef](#)]
74. Deschamps, A.; Hutchinson, C.R. Precipitation kinetics in metallic alloys: Experiments and modeling. *Acta Mater.* **2021**, *220*, 117338. [[CrossRef](#)]
75. Liu, X.M.; Wang, Q.; Zhao, C.; Li, H.P.; Wang, M.L.; Chen, D.; Wang, H.W. Formation of ordered precipitates in Al-Sc-Er-(Si/Zr) alloy from first-principles study. *J. Rare Earths* **2021**, *39*, 609–620. [[CrossRef](#)]
76. Chen, D.; Xia, C.J.; Liu, X.M.; Wu, Y.; Wang, M.L. The effect of alloying elements on the structural stability, and mechanical and electronic properties of Al₃Sc: A first-principles study. *Materials* **2019**, *12*, 1539. [[CrossRef](#)]
77. Sun, S.P.; Li, X.P.; Lei, W.N.; Wang, H.J.; Wang, X.C.; Jiang, H.F.; Li, R.X.; Jiang, Y.; Yi, D.Q. Calculation of point defect structures and bonding behavior of L1₂-Al₃Sc intermetallic based on first-principles. *Chin. J. Nonferr. Met.* **2013**, *23*, 2147–2155.
78. Peng, G.S.; Gu, Y.C.; Chen, S.Y.; Chen, K.H.; Fang, H.C.; Song, G.S. Research progress of relationship between multi-scale second phase particles and properties of Al-Zn-Mg-Cu alloys. *Rare Met. Mater. Eng.* **2021**, *50*, 775–786.
79. Deng, Y.L.; Zhang, X.M. Development of aluminium and aluminium alloy. *Chin. J. Nonferr. Met.* **2019**, *29*, 2115–2141.
80. Rometsch, P.A.; Zhang, Y.; Knight, S. Heat treatment of 7xxx series aluminium alloys—Some recent developments. *Trans. Nonferr. Met. Soc. China* **2014**, *24*, 2003–2017. [[CrossRef](#)]
81. Ye, Z.Y. Corrosion Behavior of New Aluminum Alloy and the Effect of Surface Modification. Ph.D. Thesis, Northwestern Polytechnical University, Xi'an, China, 2015.
82. Hu, H.Q. *Principle of Metal Solidification*, 2nd ed.; Machinery Industry Press: Beijing, China, 2000; pp. 190–192.
83. Bai, Q.L. Study on the Cracking Defects during Direct-Chill Casting of 7xxx Series Aluminum Alloys. Ph.D. Thesis, University of Science and Technology Beijing, Beijing, China, 2016.
84. Guo, F.B.; Zhu, B.H.; Jin, L.B.; Wang, G.J.; Yan, H.W.; Li, Z.H.; Zhang, Y.A.; Xiong, B.Q. Microstructure and mechanical properties of 7A56 aluminum alloy after solution treatment. *Rare Met.* **2021**, *40*, 168–175. [[CrossRef](#)]
85. Zhang, J.L.; Song, B.; Wei, Q.S.; Bourell, D.; Shi, Y.S. A review of selective laser melting of aluminum alloys: Processing, microstructure, property and developing trends. *J. Mater. Sci. Technol.* **2019**, *35*, 270–284. [[CrossRef](#)]
86. Wang, T.; Yin, Z.M.; Sun, Q. Effect of homogenization treatment on microstructure and hot workability of high strength 7B04 aluminium alloy. *Chin. J. Nonferr. Met.* **2007**, *2*, 335–339. [[CrossRef](#)]
87. Liu, C.Y.; Teng, G.B.; Ma, Z.Y.; Wei, L.L.; Zhang, B.; Chen, Y. Effects of Sc and Zr microalloying on the microstructure and mechanical properties of high Cu content 7xxx Al alloy. *Int. J. Min. Met. Mater.* **2019**, *26*, 1559–1569. [[CrossRef](#)]
88. Jia, M.; Zheng, Z.Q.; Gong, Z. Microstructure evolution of the 1469 Al-Cu-Li-Sc alloy during homogenization. *J. Alloys Compd.* **2014**, *614*, 131–139. [[CrossRef](#)]
89. Gazizov, M.; Teleshov, V.; Zakharov, V.; Kaibyshev, R. Solidification behaviour and the effects of homogenisation on the structure of an Al-Cu-Mg-Ag-Sc alloy. *J. Alloys Compd.* **2011**, *509*, 9497–9507. [[CrossRef](#)]
90. Manfredi, D.; Bidulský, R. Laser powder bed fusion of aluminum alloys. *Acta Metall. Slovaca.* **2017**, *23*, 276–282. [[CrossRef](#)]
91. Bidulská, J.; Bidulský, R.; Grande, M.A.; Kvačák, T. Different formation routes of pore structure in aluminum powder metallurgy alloy. *Materials* **2019**, *12*, 3724. [[CrossRef](#)]
92. Rai, R.; De, A.; Bhadeshia, H.K.D.H.; DebRoy, T. Review: Friction stir welding tools. *Sci. Technol. Weld. Joi.* **2011**, *16*, 325–342. [[CrossRef](#)]
93. Xu, F.S.; Zhang, J.; Deng, Y.L.; Zhang, X.M. Effect of snake rolling on strength, toughness and microstructure of Al-Cu-Mg alloy plate. *Chin. J. Nonferr. Met.* **2017**, *27*, 2005–2011.
94. Xia, W.J. Research on Special Rolling Techniques of Wrought Magnesium Alloy Sheet. Ph.D. Thesis, Hunan University, Hunan, China, 2010.
95. Li, S.; Qin, N.; Liu, J.; Zhang, X. Microstructure, texture and mechanical properties of AA1060 aluminum plate processed by snake rolling. *Mater. Des.* **2016**, *90*, 1010–1017. [[CrossRef](#)]
96. Zhang, T.; Wu, Y.X.; Gong, H.; Zheng, X.Z.; Jiang, S.S. Effects of rolling parameters of snake hot rolling on strain distribution of aluminum alloy 7075. *Trans. Nonferr. Met. Soc. China* **2014**, *24*, 2150–2156. [[CrossRef](#)]

97. Qin, G.H.; Yang, Y.; Li, Q.; Lin, F. Analysis and prediction of multi-pass snake hot rolling for 7075 aluminum alloy thick plate. *Opt. Precis. Eng.* **2017**, *25*, 437–446.
98. Song, M.; Liu, X.H.; Liu, X.; Liu, L.Z. Ultrafine microstructure and texture evolution of aluminum foil by asymmetric rolling. *J. Cent. S. Univ.* **2017**, *24*, 2783–2792. [[CrossRef](#)]
99. Liang, S.B. *Extrusion and Heat Treatment of Aluminum Alloy*, 1st ed.; Central South University Press: Changsha, China, 2015; pp. 470–472.
100. Feng, D.; Liu, S.D.; Han, N.M.; Chen, H.M.; Cao, W.K.; Han, Z.J. Multifactorial effects on microstructure, properties and through-thickness inhomogeneity of 7A55-RRA treated aluminum alloy thick plate. *Chin. J. Nonferr. Met.* **2019**, *29*, 1150–1160.
101. Wang, J.Y. The Mechanism Research of Strength, Toughness and Aging Stability of AA7021 Aluminum Alloy Thin Plates. Ph.D. Thesis, University of Science and Technology Beijing, Beijing, China, 2019.
102. Wang, F.F.; Meng, W.; Zhang, H.W.; Han, Z.Q. Effects of under-ageing treatment on microstructure and mechanical properties of squeeze-cast Al-Zn-Mg-Cu alloy. *Trans. Nonferr. Met. Soc. China* **2018**, *28*, 1920–1927. [[CrossRef](#)]
103. Wang, X.G.; Ma, L.Y. Microstructure and property Evolution of Al-Zn-Mg-Cu alloy with Ho addition during homogenization. *Rare Met. Mater. Eng.* **2021**, *50*, 2771–2776.
104. Zhang, K.R.; Xu, X.J.; Zhang, J. Effect of multistage solution and aging treatment on microstructure and properties of 7xxx series ultra-high strength cold extruded aluminum alloy. *Heat Treat Metal.* **2021**, *46*, 165–168.
105. Zhang, C.S.; Zhang, Z.G.; Liu, M.P.; Bao, E.C.; Chen, L.; Zhao, G.Q. Effects of single- and multi-stage solid solution treatments on microstructure and properties of as-extruded AA7055 helical profile. *Trans. Nonferr. Met. Soc. China* **2021**, *31*, 1885–1901. [[CrossRef](#)]
106. Liu, P.; Hu, L.L.; Zhang, Q.H.; Yang, C.P.; Yu, Z.S.; Zhang, J.Q.; Hu, J.M.; Cao, F.H. Effect of aging treatment on microstructure and corrosion behavior of Al-Zn-Mg aluminum alloy in aqueous solutions with different aggressive ions. *J. Mater. Sci. Technol.* **2021**, *64*, 85–98. [[CrossRef](#)]
107. Qu, M.; Tang, J.G.; Ye, L.Y.; Li, C.B.; Li, J.X.; Zhou, W.; Deng, Y.L. Comparative study on the effect of over-aging and addition of Zr on the corrosion resistance of Al-Zn-Mg alloy. *Mater. Rev.* **2020**, *34*, 2083–2087.
108. Zheng, X.; Tang, J.G.; Zhang, Y.; Chen, M.Y.; Liu, S.D.; Zhu, Y.T.; He, K.H.; Zhang, X.M. Effect of intermittent aging on mechanical properties and local corrosion properties of Al-Zn-Mg-Cu aluminum alloy thick plate. *Chin. J. Nonferr. Met.* **2022**. Available online: <http://kns.cnki.net/kcms/detail/43.1238.tg.20211022.1156.003.html> (accessed on 20 January 2022).
109. Ding, Q.W. Microstructure and Properties of Age-Hardenable Al-Mg-Zn Aluminum Alloy and the Process Optimization. Ph.D. Thesis, University of Science and Technology Beijing, Beijing, China, 2019.
110. Gokhan, O.; Ahmet, K. Properties of AA7075 aluminum alloy in aging and retrogression and reaging process. *Trans. Nonferr. Met. Soc. China* **2017**, *27*, 2357–2362.
111. Liao, B. Basic Research on Deformation Behavior and Heat Treatment Characteristics of 7055 Aluminum Alloy Thick Plate. Ph.D. Thesis, Chongqing University, Chongqing, China, 2019.
112. Jaburek, N.; Merklein, M. Influence of a retrogression and reaging (RRA)-treatment on the mechanical and microstructural characteristics of the aluminium alloy AlZn_{4.5}Mg₁. *Prod. Eng. Res. Devel.* **2015**, *9*, 161–166. [[CrossRef](#)]